Reduced Nitrosyl Polyoxomolybdates with the Hitherto Unknown Decamolybdate Y Structure: Preparation and Crystal and Electronic Structures of the Two-Electron Reduced $[Mo_{10}O_{25}(OMe)_6(NO)]^-$ and the Four-Electron Reduced $[Mo_{10}O_{24}(OMe)_7(NO)]^{2-}$

Anna Proust,*,† Francis Robert,† Pierre Gouzerh,† Qin Chen,‡ and Jon Zubieta‡

Contribution from the Laboratoire de Chimie des Métaux de Transition, URA 419, Université Pierre et Marie Curie, 4 place Jussieu, case 42, 75 252 Paris Cedex 05, France, and Department of Chemistry, Syracuse University, Syracuse, New York 13244

Received October 7, 1996[⊗]

Abstract: Reaction of either $(n\text{-}Bu_4N)_2[Mo_5O_{13}(OMe)_4(NO)\{Na(MeOH)\}]\cdot x$MeOH or $(n\text{-}Bu_4N)_3[Mo_6O_{18}(NO)]$ with various reducing agents, including $N_2H_4\cdot 2HCl$, in methanol or in a mixture of methanol and acetonitrile, yields reduced nitrosyl decamolybdates, among which $(n\text{-}Bu_4N)[Mo_{10}O_{25}(OMe)_6(NO)]$ ($(n\text{-}Bu_4N)$**II**) and two forms of $(n\text{-}Bu_4N)_2[Mo_{10}O_{24}(OMe)_7(NO)]$ ($(n\text{-}Bu_4N)_2$**IVa** and $(n\text{-}Bu_4N)_2$**IVb**) have been crystallographically characterized. **IVa**,**b** are diastereoisomers that differ in the location of methoxo groups. The molecular structures of **II** and **IV** are closely related to that of $[W_{10}O_{32}]^{4-}$, the so-called decatungstate Y, and consist of two halves of five edge-sharing octahedra connected through four quasi-linear Mo−O−Mo bridges. Besides the four electrons essentially residing at the Mo(II) center bearing the nitrosyl ligand, **II** and **IV** further accommodate two and four delocalized "blue" electrons, respectively. **II** and **IV** thus contain molybdenum atoms in three different oxidation states, Mo(II), Mo(V), and Mo(VI). On the basis of their optical spectra, they are best described as class II mixed-valence complexes according to the classification of Robin and Day. Their intimate electronic structure has been further investigated by means of extended Hückel calculations on the model compound $[Mo_{10}O_{26}(OH)_6]$. The composition of the HOMO clearly demonstrates that the "blue" electrons are circulating among the eight equatorial molybdenum sites, the delocalization being strongly favored by the quasi-linear M−O−Mo bridges.

Introduction

Polyoxometalates are molecular metal−oxygen clusters which are of fundamental and practical interest.[1−3] Their remarkable electron storage capacity—$[H_2W_{12}O_{40}]^{6-}$ can accomodate up to 32 electrons[4]!—and the electron delocalization within the oxide framework provide unique opportunities for the investigation of a number of processes which are of fundamental importance in the frame of molecular materials, *e.g.* (i) thermal and optical electron transfer,[5] (ii) interactions between delocalized and localized electrons,[6a] (iii) magnetic exchange interactions,[6b] and (iv) intramolecular energy transfer.[6c] According to Pope,[7] polyoxometalates can be divided into three types: type I, which comprises polyanions in which each metal center exhibits a single terminal oxo ligand, type II, characterized by two terminal oxo ligands *per* metallic atom, and type III, as a combination of the two former (three terminal oxo ligands should be ruled out according to Lipscomb's rule,[8] although this has occasionally been observed[9]). Only type I polyanions have proved to be reversibly reduced, that is, with minimal structural modifications.[10,11] Such reduced species, commonly referred to as "poly blues" or "heteropoly blues", have been subjected to a number of reviews.[1,12] Their features have been studied by a number of methods (*e.g.*, IR,[12c] UV−vis−near-IR,[5,10,11] ESR,[5,13] NMR,[14] photoelectron spectroscopy,[15] magnetic susceptibility stu-

† Université Pierre et Marie Curie.

‡ Syracuse University.

[⊗] Abstract published in *Advance ACS Abstracts,* April 1, 1997.

(1) Pope, M. T. *Heteropoly and Isopoly Oxometalates*; Springer-Verlag: New York, 1983.

(2) (a) Pope, M. T.; Müller A. *Angew. Chem., Int. Ed. Engl.* **1991**, *30*, 34. (b) *Polyoxometalates from Platonic Solids to Anti-Retroviral Activity*; Pope, M. T., Müller, A., Eds.; Kluwer Academic Publishers: Dordrecht, the Netherlands, 1994.

(3) Hill, C. L.; Prosser-McCartha, C. M. *Coord. Chem. Rev*. **1995**, *143*, 407.

(4) Launay, J.-P. *J. Inorg. Nucl. Chem*. **1976**, *38*, 807.

(5) (a) Che, M.; Fournier, M.; Launay, J.-P. *J. Chem. Phys.* **1979**, *71*, 1954. (b) Jeannin, Y.; Launay, J.-P.; Sanchez, C.; Livage, J.; Fournier, M. *New J. Chem.* **1980**, *4*, 587. (c) Sanchez, C.; Livage, J.; Launay, J.-P.; Fournier, M., Jeannin, Y. *J. Am. Chem. Soc*. **1982**, *104*, 3194. (d) Sanchez, C.; Livage, J.; Launay, J.-P.; Fournier, M. *J. Am. Chem. Soc.* **1983**, *105*, 6817.

(6) (a) Casan-Pastor, N.; Baker, L. C. W. In ref 2b; p. 203. (b) Coronado, E.; Gomez-Garcia, C. J. In ref 2b, p 233. (c) Yamase, T. In ref 2b, p 337.

(7) Pope, M. T. *Inorg. Chem.* **1972**, *11*, 1973.

(8) Lipscomb, W. N. *Inorg. Chem*., **1965**, *4*, 132.

(9) Chen, Q.; Zubieta, J. *Coord. Chem. Rev*. **1992**, *114*, 107.

(10) (a) Massart, R.; Hervé, G. *Rev. Chim. Min*. **1968**, *5*, 501. (b) Fruchart, J.-M.; Hervé, G.; Launay, J.-P.; Massart, R. *J. Inorg. Nucl. Chem*. **1976**, *38*. 1627.

(11) (a) Pope, M. T.; Varga, G. M., Jr. *Inorg. Chem*. **1966**, *5*, 1249. (b) Pope, M. T.; Papaconstantinou, E. *Inorg. Chem*. **1967**, *6*, 1147. (c) Papaconstantinou, E.; Pope, M. T. *Inorg. Chem*. **1967**, *6*, 1152. (d) Varga, G. M., Jr.; Papaconstantinou, E.; Pope, M. T. *Inorg. Chem.* **1970**, *9*, 662. (e) Papaconstantinou, E.; Pope, M. T. *Inorg. Chem*. **1970**, *9*, 667.

(12) (a) Pope, M. T. In *Mixed-Valence Compounds*; Brown, D. B., Ed.; D. Reidel Publishing Co. Dordrecht, The Netherlands, 1980; p 365. (b) Krebs, B. In *Transition Metal Chemistry*; Müller, A., Diemann, E., Eds.; Verlag Chemie: Weinheim, Germany, 1981; p 91. (c) Buckley, R. I.; Clark, R. J. H. *Coord. Chem. Rev.* **1985**, *65*, 167. (d) Young, C. J. *Coord. Chem. Rev.* **1989**, *96*, 89. (e) Pope, M. T. *Prog. Inorg. Chem.* **1991**, *39*, 181.

(13) (a) Altenau, J. J.; Pope, M. T.; Prados, R. A.; So, H. *Inorg. Chem.* **1975**, *14*, 417. (b) Prados, R. A.; Pope, M. T. *Inorg. Chem.* **1976**, *10*, 2547. (c) Piepgrass, K.; Barrows, J. N.; Pope, M. T. *J. Chem. Soc., Chem. Commun.* **1989**, 10.

(14) (a) Kozik, M.; Hammer, C. F.; Baker, L. C. W. *J. Am. Chem. Soc.* **1986**, *108*, 2748. (b) Kozik, M.; Hammer, C. F.; Baker, L. C. W. *J. Am. Chem. Soc.* **1986**, *108*, 7627. (c) Kirkby, J. F.; Baker, L. C. W. *J. Am. Chem. Soc.* **1995**, *117*, 10010 and references therein. (d) Duncan, D. C.; Hill, C. L. *Inorg. Chem.* **1996**, *35*, 5828.

S0002-7863(96)03514-7 CCC: $14.00

dies,[16] and X-ray diffraction[17−21]) and discussed in terms of various models.[22−24] They are best described as class II mixed-valence compounds,[25] that is with weakly trapped Mo^{5+} or W^{5+} centers. Ground-state delocalization on several addendum atoms has indeed been inferred from either ESR[5,13] or NMR studies.[14]

One of the most extensively studied polyoxometalates is the decatungstate anion, $[W_{10}O_{32}]^{4-}$ (the so-called tungstate Y).[26] This species displays electrochemically reversible reduction steps,[27] and there is retention of the structure on reduction by one or two electrons.[14d,20] It is among the most active polyoxometalates which promote alkane oxidation[28] and nanosecond[29] and picosecond[28] transient absorption studies of it have been reported. Thus, it is unfortunate that its molybdenum counterpart, $[Mo_{10}O_{32}]^{4-}$, is unknown, which precludes a comparison between the photochemical properties of these two species. The only isolated decamolybdate that has been characterized to date, $[Mo_{10}O_{34}]^{8-}$, is built up by connecting one Mo_8O_{28} unit at corners to two MoO_4 octahedra.[30] We report here the synthesis and physicochemical characterization of some derivatives of the putative $[Mo_{10}O_{32}]^{4-}$ anion, namely $[Mo_{10}O_{25}(OMe)_6(NO)]^-$ (**II**) and two isomers of $[Mo_{10}O_{24}(OMe)_7(NO)]^{2-}$ (**IVa**,**b**). These three compounds have been characterized as tetrabutylammonium salts by single-crystal X-ray analyses; they provide the first examples of a series of compounds whose structures are directly related to that $[W_{10}O_{32}]^{4-}$.[26] It is also noteworthy that only a few molybdate "poly blues" have been structurally characterized: β-$Ca_{0.5}H_6[PMo_{12}O_{40}]$,[17] β-$[H_4AsMo_{12}O_{40}]^{3-}$, α-$[H_2AsMo_{12}O_{40}]^{3-}$,[18] α-$[HPMo_{12}O_{40}]^{4-}$, $[H_3S_2Mo_{18}O_{62}]^{5-}$,[19] $[H_{1.5}W_{10}O_{32}]^{4-}$,[20] $[H_{1.8}W_{10}O_{32}]^{4-}$,[20] and $[Mo_{14}O_{46}]^{6-}$.[21]

Roman numerals, **II** for $[Mo_{10}O_{25}(OMe)_6(NO)]^-$ and **IV** for $[Mo_{10}O_{24}(OMe)_7(NO)]^{2-}$, originate from the number of added "blue electrons" as compared to the putative oxidized parent $[Mo_{10}O_{32}]^{4-}$ and do not take into account the d-electrons localized on the Mo(NO) fragment. Assuming the latter to be a $Mo(NO)^{3+}$ unit, as in all the oxonitrosyl molybdates we have previously characterized,[31−33] and taking into account charge balance considerations, $[Mo_{10}O_{25}(OMe)_6(NO)]^-$ would thus comprise seven Mo(VI) and two Mo(V) centers and will be consequently designated by **II**. On a similar basis, $[Mo_{10}O_{24}(OMe)_7(NO)]^{2-}$ would accommodate, besides a $Mo(NO)^{3+}$ unit, five Mo(VI) and four Mo(V) centers and thus will be referred to as **IV**. **IVa**,**b** designate two isomers, differing in the location of some methoxo ligands. The Mo^V centers could not be located by X-ray diffraction, which could result either from extensive electron delocalization (*vide infra*) or from a disorder among the molydenum atoms, which is very frequent in polyoxometalates. Although these species are diamagnetic, they could not be characterized by multinuclear spectroscopy. Therefore, to gain some insight into their intimate electronic structure, we have undertaken extended Hückel (EH) calculations, which lead to the conclusion that the extra "blue" electrons are delocalized among the eight equatorial molybdenum sites.

Experimental Section

Reagent-grade acetonitrile, methanol, THF, or diethyl ether and HPLC grade DMF, N_2H_4·2HCl, and VCl_3 were purchased from Aldrich and used as received. $(n\text{-}Bu_4N)_4[W_{10}O_{32}]$,[34] $[MoCl_4(MeCN)_2]$,[35] $(n\text{-}Bu_4N)_2[Mo_5O_{13}(OMe)_4(NO)\{Na(MeOH)\}]\cdot x$MeOH,[32] and $(n\text{-}Bu_4N)_3[Mo_6O_{18}(NO)]$[33] were synthesized as reported in the literature. $(n\text{-}Bu_4N)BF_4$ was prepared from $(n\text{-}Bu_4N)HSO_4$ and $NaBF_4$ and dried overnight under vacuum. When stated, methanol was distilled on magnesium methoxide.

Infrared spectra were recorded from KBr pellets on a Bio-Rad FT 165 spectrophotometer. The electronic absorption spectra were recorded on Shimadzu model UV-2101 (UV−visible) and Beckman model UV 5240 (near-IR) spectrophotometers.

The susceptibility measurements were performed on SQUID magnetometer in the 2−290 K temperature range using a 1 kOe magnetic field.

Elemental analyses were performed by the Service Central d'Analyse of the CNRS (Vernaison, France).

Synthesis of $(n\text{-}Bu_4N)[Mo_{10}O_{25}(OMe)_6(NO)]$ ($(n\text{-}Bu_4N)$II). To a solution of 0.25 mmol (0.34 g) of $(n\text{-}Bu_4N)_2[Mo_5O_{13}(OMe)_4(NO)\{Na(MeOH)\}]$ in 10 mL of hot distilled methanol was added 0.25 mmol (0.04 g) of VCl_3. The violet color immediately turned blue. After a 4 h reflux under a nitrogen atmosphere, the blue precipitate, which had formed, was collected by filtration and washed with diethyl ether. Recrystallization in a THF/MeOH mixture afforded a few dark blue crystals of $(n\text{-}Bu_4N)$**II**.

Synthesis of $(n\text{-}Bu_4N)_2[Mo_{10}O_{24}(OMe)_7(NO)]$ ($(n\text{-}Bu_4N)_2$IVa). To a brown solution of 0.5 mmol (0.8 g) of $(n\text{-}Bu_4N)_3[Mo_6O_{18}(NO)]$ in 30 mL of a 1:1 mixture of methanol and acetonitrile was added 1 mmol (0.104 g) of N_2H_4·2HCl. Upon heating to reflux, the solution developed a blue color after about one-half hour. After a 7 h reflux, the blue solution was set aside and dark blue crystals of $(n\text{-}Bu_4N)_2$**IVa** deposited within a few hours; these were filtered off after 2 days and air dried (0.14 g; yield: 22% based on Mo). Anal. Calcd for $C_{39}H_{93}Mo_{10}N_3O_{32}$: C, 22.57; H, 4.54; Mo, 46.22; N, 2.02. Found: C, 22.31; H, 4.53; Mo, 46.52; N, 2.00. IR (KBr pellet, cm^{-1}): 2963 (m), 2929 (m), 2878 (m), 2822 (w), 1659 (s) ν(NO), 1480 (m), 1384 (w), 1030 (s), 953 (vs), 783 (w), 632 (m). Visible/near-IR [MeCN; λ_{max}, nm (ϵ, mol^{-1} L cm^{-1})]: 635 (13 930), 920 (4600).

Synthesis of $(n\text{-}Bu_4N)_2[Mo_{10}O_{24}(OMe)_7(NO)]$ ($(n\text{-}Bu_4N)_2$IVb). To a violet solution of 0.25 mmol (0.34 g) of $(n\text{-}Bu_4N)_2[Mo_5O_{13}(OMe)_4(NO)\{Na(MeOH)\}]$ in 10 mL of hot, freshly distilled, methanol was

(15) Kazansky, L. P.; Launay, J.-P. *Chem. Phys. Lett.* **1977**, *51*, 242.
(16) Casan-Pastor, N.; Baker, L. C. W. *J. Am. Chem. Soc.* **1992**, *114*, 10384 and references therein.
(17) Barrows, J. N.; Jameson, G. B.; Pope, M. T. *J. Am. Chem. Soc.* **1985**, *107*, 1771.
(18) Müller, A.; Krickemeyer, E.; Penk, M.; Wittneben, V.; Döring, J. *Angew. Chem., Int. Ed. Engl.* **1990**, *29*, 88.
(19) Neier, R; Trojanowski, C.; Mattes, R. *J. Chem. Soc., Dalton Trans.* **1995**, 2521.
(20) Sasaki, Y.; Yamase, T.; Ohashi, Y.; Sasada, Y. *Bull. Chem. Soc. Jpn.* **1987**, *60*, 4285.
(21) Yamase, T. *J. Chem. Soc., Dalton Trans*. **1991**, 3055.
(22) Fournier, M.; Rocchiccioli-Deltcheff, C.; Kazansky, L. *Chem. Phys. Lett.* **1994**, *223*, 297.
(23) Borshch, S. A. *J. Mol. Struct. (THEOCHEM)* **1995**, *330*, 139.
(24) (a) Borras-Almenar, J. J.; Clemente, J. M.; Coronado, E.; Tsukerblat, B. S. *Chem. Phys.* **1995**, *195*, 1. (b) Borras-Almenar, J. J.; Clemente, J. M.; Coronado, E.; Tsukerblat, B. S. *Chem. Phys.* **1995**, *195*, 17.
(25) Robin, M. B.; Day, P. *Adv. Inorg. Chem. Radiochem.* **1967**, *10*, 248.
(26) Fuchs, J.; Hartl, H.; Schiller, W.; Gerlach, U. *Acta Crystallogr*. **1976**, *B32*, 740.
(27) (a) Boyer, M. *J. Electroanal. Chem. Interfacial Electrochem.* **1971**, *31*, 441. (b) Termes, S. C.: Pope, M. T. *Inorg. Chem.* **1978**, *17*, 500. (c) Yamase, T. *Inorg. Chim. Acta Lett.* **1983**, *76*, L23. (d) Yamase, T.; Takabayashi, N; Kaji, M. *J. Chem. Soc., Dalton Trans.* **1984**, 793. (e) Chemseddine, A.; Sanchez, C.; Livage, J.; Launay, J.-P.; Fournier M. *Inorg. Chem.* **1984**, *23*, 2609.
(28) Duncan, D. C.; Netzel, L. L.; Hill, C. L. *Inorg. Chem*. **1995**, *34*, 4640 and references therein.
(29) Yamase, T.; Usami, T. *J. Chem. Soc., Dalton Trans.* **1988**, 183.
(30) (a) Fuchs, J.; Hartl., H.; Hunnius, W.-D.; Majhour, S. *Angew. Chem., Int. Ed. Engl*. **1975**, *14*, 644. (b) Bharadwaj, P. K.; Ohashi, Y.; Sasada, Y.; Sasaki, Y.; Yamase, T. *Acta Crystallogr., Sect. C* **1986**, *C42*, 545. (c) Garin, J. L.; Costamagna, J. A. *Acta Crystallogr., Sect. C* **1988**, *C44*, 779.
(31) (a) Proust, A.; Gouzerh, P.; Robert, F. *J. Chem. Soc., Dalton Trans.* **1994**, 825. (b) Proust, A.; Horner, O.; Villanneau, R; Gouzerh, P. *New J. Chem.* **1996**, *20*, 643.
(32) (a) Gouzerh, P.; Jeannin, Y.; Proust, A.; Robert, F. *Angew. Chem., Int. Ed. Engl.* **1989**, *28*, 1363. (b) Proust, A.; Gouzerh, P.; Robert, F. *Inorg. Chem.* **1993**, *32*, 5291.
(33) (a) Proust, A.; Thouvenot, R.; Robert, F.; Gouzerh, P. *Inorg. Chem.* **1993**, *32*, 5299. (b) Proust, A; Thouvenot, R; Roh, S.-G.; Yoo, J.-K.; Gouzerh, P. *Inorg. Chem.* **1995**, *34*, 4106.
(34) Fournier M. *Inorg. Synth.* **1990**, *27*, 81.
(35) Dilworth, J. R.; Richards, R. L. *Inorg. Synth.* **1980**, *20*, 120.

Table 1. Crystal Data and Data Collection and Refinement Parameters for (n-Bu_4N)[$Mo_{10}O_{25}(OCH_3)_6(NO)$] (($n$-$Bu_4N$)**II**) and ($n$-$Bu_4N)_2[Mo_{10}O_{24}(OCH_3)_7(NO)]$ ((n-$Bu_4N)_2$**IVa,b**)

	(n-Bu_4N)**II**	(n-$Bu_4N)_2$**IVa**	(n-$Bu_4N)_2$**IVb**
formula	$C_{22}H_{54}Mo_{10}N_2O_{32}$	$C_{39}H_{93}Mo_{10}N_3O_{32}$	$C_{39}H_{93}Mo_{10}N_3O_{32}$
fw	1818.07	2075.58	2075.58
T, K	298	298	298
diffractometer	CAD4F Enraf Nonius	CAD4F Enraf Nonius	AFC5S Rigaku
λ (Mo Kα), Å	0.71069	0.71069	0.71073
a, Å	11.538(4)	11.620(2)	11.697(4)
b, Å	25.151(5)	24.332(5)	24.398(4)
c, Å	17.232(4)	24.847(3)	24.776(4)
β, deg	95.58(3)	96.75(1)	96.89(2)
V, Å^3	4976 (11)	6976(5)	7020(12)
Z	4	4	4
crystal system	monoclinic	monoclinic	monoclinic
space group	$P2_1/n$	$P2_1/n$	$P2_1/n$
systematic absences	$0k0$, $k = 2n + 1$, $h0l$, $h + l = 2n+1$	$0k0$, $k = 2n + 1$, $h0l$, $h + l = 2n + 1$	$0k0$, $k = 2n + 1$, $h0l$, $h + l = 2n + 1$
D_{calcd}, g cm^{-3}	2.43	1.98	1.96
μ(Mo Kα)	24.63	17.70	17.59
scan mode	$\omega/2\theta$	$\omega/2\theta$	ω
scan width, deg	$0.8 + 0.345 \tan\theta$	$0.8 + 0.345 \tan\theta$	$1.5 + 0.30 \tan\theta$
2θ range, deg	1−50	1−50	1−45
range hkl collected	−13 to 13, 0−29, 0−20	−12 to 12, 0−28, 0−27	0−12, 0−25, −26 to 26
no. of reflns collected	9211	9130	10148
no. of unique reflns	8756	8859	9446
no. of reflns with $I > 3\sigma(I)$	5025	3688	3306
absorption correction	Difabs[a] (min, 0.78; max, 1.19)	Difabs[a] (min, 0.81; max, 1.17)	Ψ-scans
least-squares params	591	757	388
goodness of fit	2.66	2.71	1.60
$R(F_o)$[b]	0.049	0.055	0.062
$R_w(F_o)$	0.052	0.060	0.064

[a] Reference 38. [b] $R = \sum||F_o| - |F_c||/\sum|F_o|$; $R_w = (\sum w(|F_o| - |F_c|)^2/\sum w|F_o|^2)^{1/2}$.

added, under nitrogen, 0.25 mmol (0.08 g) of [$MoCl_4(MeCN)_2$]. The resulting blue solution was boiled under reflux for 7 h, after which time a dark blue precipitate (0.15 g) was separated and washed with diethyl ether. Dark blue crystals of (n-$Bu_4N)_2$**IVb** suitable for X-ray analysis were grown from a THF/Et_2O mixture.

Electrochemistry. All measurements were carried out in DMF, under argon, at room temperature, by using a standard three-electrode cell, which consisted of the working electrode, an auxiliary platinum electrode, and an aqueous saturated calomel electrode (SCE) equipped with a double junction. Solution concentrations were *ca.* 1 mM for the compound under study and 0.1 M for the supporting electrolyte, (n-Bu_4N)BF_4. Polarograms were recorded at a rotating platinum electrode or at a dropping mercury electrode on a Tacussel PRG3 device, at the rate of 0.15 V min^{-1}. Cyclic voltamograms were recorded at a carbon electrode on a PAR 273 instrument, at the rate of 0.1 V s^{-1}.

X-ray Crystallographic Studies. Relevant crystal data, data collection, and refinement parameters for compounds (n-Bu_4N)**II**, (n-$Bu_4N)_2$**IVa**, and (n-$Bu_4N)_2$**IVb** are summarized in Table 1. The intensity data were collected, at room temperature, on either a CAD4 Enraf-Nonius or a Rigaku AFC5S diffractometer, using graphite-monochromated Mo Kα radiation. Accurate cell parameters and the orientation matrix were obtained from a least-squares fit of 25 automatically centered reflections of high θ. Reference reflections were periodically monitored for intensity and orientation control; no crystal decay was observed. Intensities were corrected for Lorentz and polarization effects, and only those with $I > 3\sigma(I)$ were retained for calculations. The structures were solved by direct methods,[36] which allowed the location of the molybdenum atoms and some of the oxo ligands, and subsequent electron density maps. Neutral-atom scattering factors were used, and anomalous dispersion corrections were included.[37] An empirical absorption correction was applied using DIFABS[38] for (n-Bu_4N)**II** and (n-$Bu_4N)_2$**IVa**, while that for (n-$Bu_4N)_2$**IVb** was based on Ψ-scans.

The locations of the methoxo ligands were determined with special attention. The procedure followed will be detailed for **II**. Careful examination of electron density difference maps unambiguously revealed that O12, O13, O14, O15, O113, O114, and O115 must bear carbon atoms, while O112 and all other bridging oxygen atoms do not. However, two refinement cycles resulted in nonhomogeneous isotropic thermal parameters: 0.077, 0.049, 0.064, 0.059, 0.283, 0.115, and 0.145, respectively. The values for O113 and, to a lesser extent, for O114 and O115 were clearly indicative of partial occupation factors. Consequently, isotropic thermal parameters and occupation factors for C113, C114, and C115 were refined by routine least-squares methods. The resulting occupation factors of 0.45, 0.85, and 0.70, respectively, were then fixed and the thermal parameters independently refined. Thus, it appears that **II** contains six methoxo ligands, two of which are disordered on three sites. Following the same treatment, **IVa** was found to accommodate seven methoxo ligands, lying on sites 12, 13, 14, 15, 112, 113, 114, and 115, one of which is disordered on two sites as C112 and C114 were assigned occupation factors of 0.55 and 0.45, respectively. In common with **IVa**, **IVb** also displays seven methoxo ligands, but is unaffected by disorder. In this instance, in addition to sites 12, 13, 14, 15, 114, and 115, an equatorial site, namely 145, is involved. As the presence of methoxo instead of oxo ligands is clearly reflected in the geometric parameters (*vide infra*), the geometry around each oxygen atom was carefully inspected.

Hydrogen atoms were placed in idealized positions for (n-$Bu_4N)_2$**IVb** but were not included in the model for **II** and **IVa**. They were isotropically refined and then introduced as fixed contributions in final refinements. All non-hydrogen atoms in **II** and **IVa** were given anisotropic temperature factors, with the exception of those of the carbon atoms with partial occupation factors. Only the molybdenum atoms in **IVb** were anisotropically refined. Refinements were carried out by large block matrix least-square procedures. All computations were performed using the CRYSTALS version for PC[39] or SHELXTL.[36] Selected bond lengths and angles are listed in Tables 2 and 3, respectively.

The numbering schemes for the $[Mo_{10}O_{31-x}(OMe)_x(NO)]^{n-}$ anions follow that previously adopted for the $[Mo_5O_{13}(OMe)_4(NO)]^{3-}$ unit.[32] The molybdenum atom bearing the nitrosyl ligand, N1O1, was labeled Mo1, while the adjacent molybdenum atoms were numbered from Mo2

(36) Sheldrick, G. M. *SHELXS 86, A Program for Crystal Structure Determination*, University of Göttingen, 1986.

(37) *International Tables for X-Ray Crystallography*; Kynoch: Birmingham, U.K., 1974; Vol. IV, pp 149−150.

(38) Walker, N.; Stuart, D. *Acta Crystallogr., Sect. A* **1983**, *A39*, 158.

Table 2. Selected Bond Lengths (Å) for $(NBu_4)[Mo_{10}O_{25}(OCH_3)_6(NO)]$ ((NBu_4)**II**) and $(NBu_4)_2[Mo_{10}O_{24}(OCH_3)_7(NO)]$ ($(NBu_4)_2$**IVa,b**)

	II	IVa	IVb		II	IVa	IVb
Mo1−N1	1.77(1)	1.73(3)	1.74(2)	Mo101−O110	2.224(9)	2.19(2)	2.20(2)
Mo1−O10	2.123(8)	2.11(2)	2.13(2)	Mo101−O101	1.69(1)	1.67(2)	1.67(2)
Mo1−O12	2.013(9)	2.02(2)	2.02(2)	Mo101−O112	1.80(1)	1.89(2)	1.87(2)
Mo1−O13	2.00(1)	1.97(2)	1.99(2)	Mo101−O113	1.91(1)	2.03(2)	1.89(2)
Mo1−O14	2.013(9)	2.02(2)	1.96(2)	Mo101−O114	1.98(1)	1.84(2)	1.98(2)
Mo1−O15	1.987(9)	1.99(2)	1.99(2)	Mo101−O115	2.05(1)	1.99(2)	2.04(2)
Mo2−O10	2.360(8)	2.37(2)	2.39(2)	Mo102−O2	1.878(9)	1.89(2)	1.90(2)
Mo2−O12	2.139(9)	2.16(2)	2.15(2)	Mo102−O110	2.388(9)	2.34(1)	2.47(2)
Mo2−O2	1.852(9)	1.85(2)	1.85(2)	Mo102−O112	2.04(1)	2.04(2)	2.07(2)
Mo2−O22	1.67(1)	1.67(2)	1.67(2)	Mo102−O122	1.67(1)	1.66(2)	1.69(2)
Mo2−O23	1.901(8)	1.90(1)	1.93(2)	Mo102−O123	1.906(9)	1.92(1)	1.91(2)
Mo2−O24	1.896(8)	1.93(1)	1.89(2)	Mo102−O124	1.890(9)	1.93(1)	1.88(2)
Mo3−O10	2.336(8)	2.33(1)	2.32(2)	Mo103−O3	1.887(9)	1.90(2)	1.89(2)
Mo3−O13	2.152(9)	2.19(2)	2.15(2)	Mo103−O110	2.359(9)	2.30(2)	2.44(2)
Mo3−O23	1.896(9)	1.89(2)	1.91(2)	Mo103−O113	2.07(1)	2.14(2)	2.07(2)
Mo3−O3	1.86(1)	1.83(2)	1.86(2)	Mo103−O123	1.90(1)	1.90(1)	1.93(2)
Mo3−O32	1.668(9)	1.68(2)	1.67(2)	Mo103−O132	1.66(1)	1.68(2)	1.66(2)
Mo3−O35	1.897(9)	1.90(2)	1.90(2)	Mo103−O135	1.92(1)	1.92(2)	1.89(2)
Mo4−O10	2.363(8)	2.38(1)	2.38(2)	Mo104−O4	1.875(9)	1.89(2)	1.93(2)
Mo4−O14	2.153(9)	2.17(2)	2.17(2)	Mo104−O110	2.288(9)	2.38(2)	2.24(2)
Mo4−O24	1.905(9)	1.89(1)	1.91(2)	Mo104−O114	2.10(1)	2.07(2)	2.12(2)
Mo4−O4	1.863(9)	1.85(2)	1.83(2)	Mo104−O124	1.906(9)	1.92(1)	1.92(2)
Mo4−O42	1.657(9)	1.64(2)	1.67(2)	Mo104−O142	1.67(1)	1.66(2)	1.67(2)
Mo4−O45	1.907(8)	1.86(2)	1.88(2)	Mo104−O145	1.90(1)	1.89(2)	1.99(2)
Mo5−O10	2.317(8)	2.34(2)	2.32(2)	Mo105−O5	1.893(9)	1.90(2)	1.94(2)
Mo5−O15	2.186(9)	2.17(2)	2.18(2)	Mo105−O110	2.253(9)	2.31(2)	2.24(2)
Mo5−O35	1.899(9)	1.90(1)	1.91(2)	Mo105−O115	2.14(1)	2.12(2)	2.10(2)
Mo5−O45	1.893(9)	1.92(2)	1.95(2)	Mo105−O135	1.89(1)	1.92(2)	1.89(2)
Mo5−O5	1.862(9)	1.85(2)	1.82(2)	Mo105−O145	1.90(1)	1.87(2)	1.99(2)
Mo5−O52	1.67(1)	1.66(2)	1.65(2)	Mo105−O152	1.67(1)	1.69(2)	1.67(2)
N1−O1	1.17(1)	1.21(3)	1.22(3)	O112−C112		1.3(1)	
O12−C12	1.44(2)	1.43(3)	1.43(4)	O113−C113	1.44(5)	1.46(4)	
O13−C13	1.45(2)	1.46(3)	1.43(4)	O114−C114	1.49(3)	1.5(1)	1.42(5)
O14−C14	1.44(2)	1.44(3)	1.44(4)	O115−C115	1.35(3)	1.50(5)	1.41(5)
O15−C15	1.44(2)	1.48(3)	1.41(5)	0145−C145			1.51(5)

through Mo5. Since the anions can be built from two "Mo_5" units connected by quasi-linear Mo−O−Mo bridges, the numbering scheme in the "lower" half was derived from that of the "upper" one by adding 100 to each basic number. Connecting oxygen atoms between Mo*i* and Mo10*i* were labeled O*i*. Terminal oxygen atoms (O_t) were labeled O*i*2, where *i* is the number of the molydenum atom, with the exception of that on Mo101, which was labeled O101. Bridging oxygen atoms (O_b) were labeled O*ij*, where *i* and *j* are the numbers of the bridged molybdenum atoms, and central oxygen atoms (O_c) were labeled O10 and O110. Finally, carbon atoms were assigned the same labels as the oxygen atoms to which they are linked.

Extended Hückel Calculations. The isolated anion $[Mo_{10}O_{25}(OMe)_6(NO)]^-$ (**II**) and the hypothetical species $[Mo_{10}O_{26}(OMe)_6]$, $[Mo_{10}O_{32}]^{4-}$, and $[Mo(NO)(OMe)_4O]^{3-}$ were subjected to EH calculations.[40] To facilitate the calculations and to avoid accidental orbital splittings, geometric data derived from the X-ray crystallographic study of $(n\text{-}Bu_4N)[Mo_{10}O_{25}(OMe)_6(NO)]$ ($(n\text{-}Bu_4N)$**II**) were constrained to approximate D_{4h} symmetry. Cartesian coordinates were used. Reference axes are as followed: the plane through the four O*i* atoms was taken as $z = 0$, and the *x* and *y* axes, respectively, lie along the O3−O4 and O5−O2 vectors. Methyl groups were replaced by hydrogen atoms and forced in the Mo1−O1*i*−Mo*i* or Mo101−O11*i*−Mo10*i* planes. Only O114 and O115 were protonated, neglecting the disorder affecting O113, O114, and O115 in **II** (*vide supra*). The Mo(NO) fragment was constrained along the *z* axis. Strictly speaking, the idealized $[Mo_{10}O_{25}(OH)_6(NO)]^-$ anion has C_s, not D_{4h}, symmetry. EH calculations were also performed on the model $[Mo_{10}O_{26}(OH)_6]$ derived from $[Mo_{10}O_{25}(OH)_6(NO)]^-$ by substitution of a MoO^{4+} unit for the $Mo(NO)^{3+}$ unit. Finally, to get more accurate Coulombic integrals, the valence shell ionization potentials for the formally Mo(VI) and Mo(II) centers were tentatively derived from charge iterations on $[Mo_{10}O_{32}]^{4-}$ and $[Mo(NO)(OH)_4O]^{3-}$, respectively. Geometrical parameters for $[Mo_{10}O_{32}]^{4-}$ have been approximated by those of $[W_{10}O_{32}]^{4-}$ [26] and again constrained to D_{4h} symmetry, and those of $[Mo(NO)(OH)_4O]^{3-}$ taken as in the corresponding part of $[Mo_{10}O_{25}(OH)_6(NO)]^-$. The Cartesian coordinates for $[Mo_{10}O_{25}(OH)_6(NO)]^-$ and $[Mo_{10}O_{32}]^{4-}$ are given in Figure 1.

The Hückel parameters were taken from Hoffmann's work[41] and are listed in Table 4. The energy of −12.3 eV for Mo d orbitals is more appropriate to Mo(VI) or Mo(V) than the value of −10.5 eV, which refers to molybdenum in low oxidation states. For d orbitals, a linear combination of two Slater-type orbitals was used, as usual. The Wolfsberg−Helmholtz coefficient was set to 1.75.

Results

Syntheses. Reduced polyanions can be generally prepared by electrolysis of their respective oxidized parents. This procedure results in good yields and high selectivity, unless decomposition or disproportionation occurs. However, it requires the availability of the parent anion. The chemical reduction described here thus provides the only way to reduced derivatives of the hitherto unknown anion $[Mo_{10}O_{32}]^{4-}$. The

(39) (a) Watkin, D. J.; Carruthers, J. R.; Betteridge, P. W. *Crystals User Guide*; Chemical Crystallography Laboratory, University of Oxford: Oxford, U.K., 1992. (b) Pearce, L. J.; Watkin, D. J. *CAMERON*; Chemical Crystallography Laboratory, University of Oxford: Oxford, U.K., 1992.

(40) FORTICON 8, QCPE 344, Indiana University, Bloomington, IN.

(41) (a) Wheeler, R. A.; Whangbo, M.-H.; Hughbanks, T.; Hoffmann, R.; Burdett, J. K.; Albright, J. A. *J. Am. Chem. Soc.* **1986**, *108*, 2222. (b) Summerville, R. H.; Hoffmann, R. *J. Am. Chem. Soc.* **1976**, *98*, 7240.

(42) Alvarez, S. Personal communication, 1989.

Table 3. Selected Bond Angles (deg) for $(NBu_4)[Mo_{10}O_{25}(OCH_3)_6(NO)]$((NBu$_4$)**II**) and $(NBu_4)_2[Mo_{10}O_{24}(OCH_3)_7(NO)]$ ((NBu$_4$)$_2$**IVa,b**)

	II	**IVa**	**IVb**		**II**	**IVa**	**IVb**
N1−Mo1−O10	178.5(5)	177.7(9)	178.3(9)	O110−Mo101−O101	168.8(5)	170.2(8)	172.0(8)
N1−Mo1−O12	97.6(5)	99.3(9)	97.(1)	O110−Mo101−O112	82.3(4)	78.6(7)	82.9(7)
O10−Mo1O12	81.1(3)	81.8(6)	81.5(7)	O101−Mo101−O112	108.7(5)	105.7(9)	104.1(9)
N1−Mo1−O13	100.3(5)	100.9(10)	99.(1)	O110−Mo101−O113	79.7(4)	76.7(6)	81.7(7)
O10−Mo1−O13	80.3(3)	81.0(6)	79.6(7)	O101−Mo101−O113	101.4(5)	94.5(9)	101.4(9)
O12−Mo1−O13	87.2(4)	90.5(7)	88.5(7)	O112−Mo101−O113	94.8(5)	86.6(7)	94.1(8)
N1−Mo1−O14	97.7(5)	95.8(10)	100.(1)	O110−Mo101−O114	76.7(4)	81.5(7)	100.1(9)
O10−Mo1−O14	81.5(3)	82.2(6)	81.0(7)	O101−Mo101−O114	100.0(5)	106.7(9)	75.9(7)
O12−Mo1−O14	86.6(4)	86.4(6)	88.3(7)	O112−Mo101−O114	91.2(5)	93.9(7)	89.1(8)
O13−Mo1−O14	161.5(4)	163.2(7)	160.6(7)	O113−Mo101−O114	154.6(4)	157.7(7)	156.8(8)
N1−Mo1−O15	99.8(5)	98.4(9)	101.(1)	O110−Mo101−O115	74.3(4)	78.2(6)	74.4(7)
O10−Mo1−O15	81.5(3)	80.4(6)	80.6(7)	O101−Mo101−O115	94.6(5)	96.1(8)	98.3(9)
O12−Mo1−O15	162.5(4)	162.1(7)	162.0(8)	O112−Mo101−O115	156.5(4)	155.5(7)	157.1(8)
O13−Mo1−O15	90.8(4)	89.0(7)	88.8(7)	O113−Mo101−O115	83.5(5)	80.5(6)	86.3(7)
O14−Mo1−O15	90.0(4)	89.0(7)	88.3(7)	O114−Mo101−O115	81.3(5)	90.4(7)	82.0(7)
O10−Mo2−O12	73.2(3)	73.3(6)	73.1(6)	O2−Mo102−O110	90.9(3)	92.6(6)	92.8(7)
O10−Mo2−O2	93.9(4)	95.0(6)	95.7(7)	O2−Mo102−O112	164.4(4)	165.0(7)	165.3(7)
O12−Mo2−O2	167.1(4)	168.3(6)	168.8(7)	O110−Mo102−O112	73.5(3)	72.4(6)	72.5(6)
O10−Mo2−O22	163.7(4)	161.4(7)	161.8(8)	O2−Mo102−O122	101.9(5)	101.0(8)	100.6(8)
O12−Mo2−O22	90.5(5)	88.1(7)	88.7(8)	O110−Mo102−O122	167.2(4)	166.4(7)	166.5(8)
O2−Mo2−O22	102.4(5)	103.6(8)	102.6(8)	O112−Mo102−O122	93.7(5)	94.0(7)	94.1(8)
O10−Mo2−O23	74.8(3)	73.9(6)	74.3(6)	O2−Mo102−O123	90.2(4)	91.0(6)	91.7(7)
O12−Mo2−O23	86.3(4)	86.1(6)	84.2(7)	O110−Mo102−O123	75.4(4)	74.8(6)	76.1(6)
O2−Mo2−O23	91.3(4)	91.4(7)	92.7(7)	O112−Mo102−O123	85.4(4)	85.5(7)	85.7(7)
O22−Mo2−O23	103.7(4)	106.0(8)	103.6(8)	O2−Mo102−O124	90.9(4)	89.8(6)	89.4(7)
O10−Mo2−O24	75.6(3)	75.2(6)	75.1(6)	O110−Mo102−O124	74.4(4)	76.5(6)	72.9(7)
O12−Mo2−O24	85.4(4)	82.9(6)	85.3(7)	O112−Mo102−O124	85.6(4)	86.4(7)	85.4(7)
O2−Mo2−O24	90.5(4)	93.5(7)	92.7(7)	O122−Mo102−O123	104.6(5)	104.5(7)	103.9(8)
O22−Mo2−O24	104.7(4)	102.5(8)	104.8(8)	O122−Mo102−O124	104.8(5)	103.5(7)	106.3(9)
O23−Mo2−O24	150.4(4)	149.0(7)	149.4(7)	O123−Mo102−O124	149.7(4)	151.3(6)	149.0(8)
O10−Mo3−O13	72.5(3)	72.0(6)	72.2(6)	O3−Mo103−O110	93.0(4)	94.7(6)	92.6(7)
O10−Mo3−O23	75.5(3)	74.9(6)	76.2(6)	O3−Mo103−O113	166.4(4)	167.0(6)	165.1(7)
O13−Mo3−O23	83.8(4)	84.8(7)	83.8(6)	O110−Mo103−O113	73.4(4)	72.3(6)	72.6(6)
O10−Mo3−O3	95.2(4)	96.6(6)	96.0(7)	O3−Mo103−O123	91.6(4)	90.8(6)	89.3(7)
O13−Mo3−O3	167.6(4)	168.6(6)	168.2(7)	O110−Mo103−O123	76.2(3)	76.2(6)	76.6(7)
O23−Mo3−O3	91.9(4)	93.1(7)	93.6(7)	O113−Mo103−O123	85.7(4)	86.8(6)	85.7(7)
O10−Mo3−O32	162.3(4)	160.4(7)	162.1(7)	O3−Mo103−O132	100.5(5)	101.7(8)	99.0(8)
O13−Mo3−O32	89.9(4)	88.4(7)	89.9(7)	O110−Mo103−O132	166.4(4)	163.5(8)	168.3(8)
O23−Mo3−O32	104.5(4)	105.4(8)	102.8(8)	O113−Mo103−O132	93.1(5)	91.3(8)	95.8(8)
O3−Mo3−O32	102.4(5)	102.9(8)	101.9(8)	O123−Mo103−O132	104.8(4)	104.8(8)	105.3(8)
O10−Mo3−O35	74.0(3)	73.7(6)	74.2(6)	O3−Mo103−O135	90.2(4)	91.4(7)	90.6(7)
O13−Mo3−O35	86.2(4)	84.5(6)	84.5(7)	O110−Mo103−O135	74.4(4)	76.3(6)	73.1(6)
O23−Mo3−O35	149.5(4)	148.6(6)	150.2(7)	O113−Mo103−O135	85.7(4)	85.0(6)	86.7(7)
O3−Mo3−O35	91.8(4)	91.7(7)	92.3(7)	O123−Mo103−O135	150.5(4)	152.5(7)	149.6(7)
O32−Mo3−O35	104.3(5)	103.6(8)	104.5(8)	O132−Mo103−O135	103.7(5)	101.6(8)	104.7(8)
O10−Mo4−O14	73.4(3)	73.3(6)	71.4(6)	O4−Mo104−O110	93.2(4)	93.0(6)	95.3(7)
O10−Mo4−O24	75.4(3)	75.7(6)	75.0(6)	O4−Mo104−O114	166.4(4)	165.5(7)	167.5(7)
O14−Mo4−O24	85.0(4)	83.7(6)	84.8(6)	O110−Mo104−O114	73.2(4)	72.6(6)	72.6(6)
O10−Mo4−O4	95.1(4)	95.6(6)	96.7(7)	O4−Mo104−O124	90.9(4)	91.4(7)	92.2(7)
O14−Mo4−O4	168.4(4)	168.9(6)	168.0(7)	O110−Mo104−O124	76.6(4)	75.7(6)	78.2(7)
O24−Mo4−O4	91.0(4)	92.8(7)	93.1(7)	O114−Mo104−O124	86.0(4)	86.6(6)	88.0(7)
O10−Mo4−O42	161.9(4)	161.0(8)	160.1(8)	O4−Mo104−O142	102.3(5)	100.7(8)	101.8(8)
O14−Mo4−O42	88.7(4)	87.8(8)	88.7(8)	O110−Mo104−O142	164.5(4)	166.4(8)	162.5(8)
O24−Mo4−O42	105.9(4)	103.1(8)	104.3(8)	O114−Mo104−O142	91.3(5)	93.8(8)	90.2(8)
O4−Mo4−O42	102.9(4)	103.4(8)	103.2(8)	O124−Mo104−O142	103.3(5)	103.6(8)	104.4(9)
O10−Mo4−O45	74.2(3)	74.2(6)	74.7(7)	O4−Mo104−O145	90.1(4)	89.7(7)	88.5(7)
O14−Mo4−O45	86.7(4)	86.4(6)	83.3(7)	O110−Mo104−O145	75.1(4)	73.1(6)	76.1(7)
O24−Mo4−O45	149.5(4)	149.9(6)	149.6(7)	O114−Mo104−O145	86.5(4)	84.7(7)	85.9(7)
O4−Mo4−O45	91.3(4)	91.6(7)	92.8(7)	O124−Mo104−O145	151.7(4)	148.8(7)	154.2(8)
O42−Mo4−O45	103.2(4)	104.8(8)	103.3(8)	O142−Mo104−O145	104.2(5)	106.8(8)	100.6(8)
O10−Mo5−O15	73.1(3)	71.9(6)	72.6(6)	O5−Mo105−O110	95.1(4)	95.2(6)	95.0(6)
O10−Mo5−O35	74.4(3)	73.4(6)	74.2(6)	O5−Mo105−O115	167.2(4)	168.2(6)	167.4(7)
O15−Mo5−O35	85.2(4)	84.8(6)	84.8(7)	O110−Mo105−O115	72.1(4)	73.2(5)	72.5(6)
O10−Mo5−O45	75.5(3)	74.2(6)	75.0(6)	O5−Mo105−O135	91.3(4)	90.7(7)	90.3(7)
O15−Mo5−O45	85.4(4)	84.8(6)	84.0(7)	O110−Mo105−O135	77.4(4)	76.2(6)	77.9(7)
O35−Mo5−O45	149.9(4)	147.6(6)	149.1(7)	O115−Mo105−O135	85.8(4)	85.0(6)	86.0(7)
O10−Mo5−O5	96.4(4)	96.8(6)	97.1(7)	O5−Mo105−O145	90.6(4)	91.4(7)	90.1(7)
O15−Mo5−O5	169.5(4)	168.7(7)	169.6(7)	O110−Mo105−O145	76.0(4)	75.4(6)	76.1(7)
O35−Mo5−O5	92.4(4)	93.1(7)	93.4(7)	O115−Mo105−O145	86.6(4)	87.4(7)	86.0(7)
O45−Mo5−O5	91.6(4)	91.3(7)	92.5(7)	O135−Mo105−O145	153.4(4)	151.6(7)	153.9(7)
O10−Mo5−O52	160.7(4)	161.4(7)	160.7(8)	O5−Mo105−O152	102.3(5)	102.0(8)	100.6(8)
O15−Mo5−O52	87.6(4)	89.5(7)	88.1(8)	O110−Mo105−O152	162.6(5)	162.8(7)	163.9(8)
O35−Mo5−O52	104.1(5)	104.3(7)	104.0(8)	O115−Mo105−O152	90.5(5)	89.6(7)	91.9(9)
O45−Mo5−O52	103.9(5)	106.1(7)	104.3(8)	O135−Mo105−O152	103.1(5)	101.7(8)	106.0(9)
O5−Mo5−O52	102.9(5)	101.8(8)	102.2(8)	O145−Mo10−O152	102.5(5)	105.6(8)	99.5(9)
Mo1−N1−O1	178.0(14)	177.7(28)	175(2)				

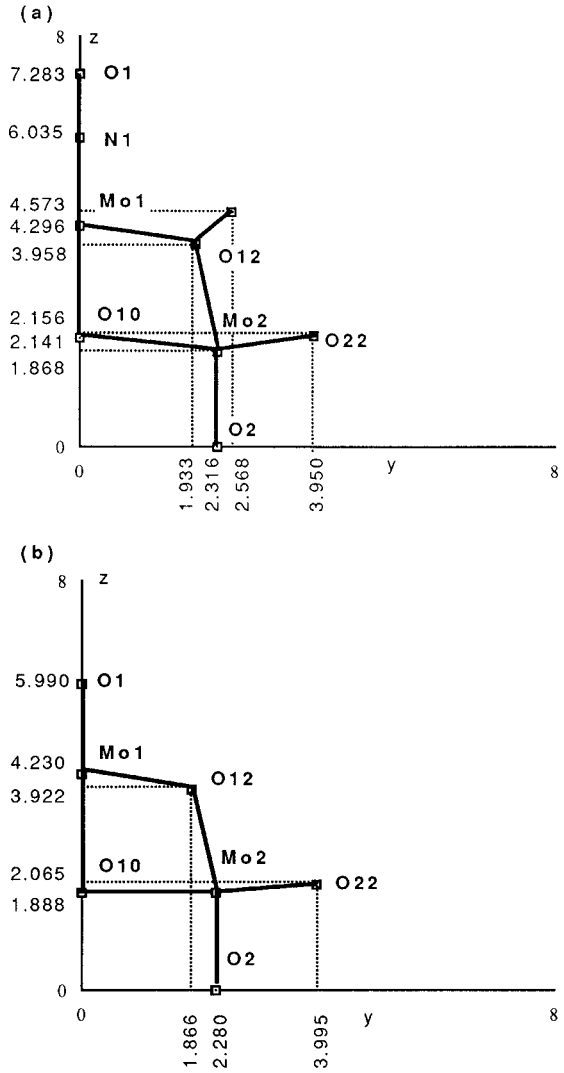

Figure 1. Cartesian coordinates used in EH calculations for the hypothetical $[Mo_{10}O_{25}(OH)_6(NO)]^-$ (a) and $[Mo_{10}O_{32}]^{4-}$ (b) anions. Structural data for $[Mo_{10}O_{32}]^{4-}$ have been approximated by those of $[W_{10}O_{32}]^{4-}$.[26]

Table 4. Atomic Parameters Used in Extended Hückel Calculations

orbitals		H_{ii},[a] eV	ζ_1[a]	ζ_2[a]	$c_1 = c_2$[a]	A[b]	B[b]	C[b]
H	s	−13.60	1.30			13.618	27.18	13.6
N	s	−26.00	1.95			0.0	13.7	26.4
	p	−13.40	1.95			0.0	13.7	13.4
O	s	−32.30	2.27			0.0	15.2	33.0
	p	−14.80	2.27			0.0	15.2	16.4
Mo	s	−9.66	1.96			1.35	5.64	6.57
	p	−6.36	1.90			1.97	2.96	4.20
	d	−12.30	4.54	1.90	0.5899	1.83	8.16	8.39

[a] Reference 41a. [b] Reference 42.

method has its drawbacks: reacting $(n\text{-Bu}_4N)_2[Mo_5O_{13}(OMe)_4(NO)\{Na(MeOH)\}]$ with VCl_3 or $[MoCl_4(MeCN)_2]$ results in mixtures of products, as revealed by the observation of complex polarograms with, notably, a mixed anodic/cathodic wave for the crude dark-blue precipitates. That recrystallization has given $(n\text{-Bu}_4N)[Mo_{10}O_{25}(OMe)_6(NO)]$ ((*n*-Bu$_4$N)**II**) in the first case and $(n\text{-Bu}_4N)_2[Mo_{10}O_{24}(OMe)_7(NO)]$ ((*n*-Bu$_4$N)$_2$**IVb**) in the second is probably fortuitous, and it is more likely that both crude precipitates contain a mixture of (*n*-Bu$_4$N)**II** and (*n*-Bu$_4$N)$_2$**IVb**, and possibly other species. The synthetic procedure was improved through the reduction of $(n\text{-Bu}_4N)_3[Mo_6O_{18}(NO)]$ by $N_2H_4\cdot 2HCl$ in a mixture of methanol and acetonitrile, and analytically pure $(n\text{-Bu}_4N)_2[Mo_{10}O_{24}(OMe)_7(NO)]$ ((*n*-Bu$_4$N)$_2$**IVa**) was reproducibly obtained in this way, albeit in moderate yield, which is not unanticipated owing to the large structural rearrangements involved in the formation of **IVa** from $[Mo_6O_{18}(NO)]^{3-}$. Our attempts to improve the yield in **IVa**, either by varying the reaction time or the amount of solvent or by lowering the amount of $N_2H_4\cdot 2HCl$, have, up to now, failed. The reaction does not occur in pure acetonitrile, as could have been anticipated from the molecular formula of **IVa**. Acetonitrile was nevertheless systematically added to the reactant mixture to ensure the solubilization of the product and to favor its crystallization. The lowering of the total cluster charge resulting from the incorporation of methoxo ligands in the molecular structure of these reduced decamolybdates parallels the effect of protonation which often accompanies the reduction of polyoxometalates in aqueous solution. $(n\text{-Bu}_4N)_2[Mo_5O_{13}(OMe)_4(NO)\{Na(MeOH)\}]$ also reacts with $N_2H_4\cdot 2HCl$ in methanol to give a few small dark blue crystals. Although their elemental analysis is not in agreement with either (*n*-Bu$_4$N)**II** or (*n*-Bu$_4$N)$_2$**IV**, they very probably belong to the same family of compounds, as inferred from their IR spectrum and their polarogram. When the amount of $N_2H_4\cdot 2HCl$ is lowered, the brown compound $(n\text{-Bu}_4N)_2[Mo_{10}O_{20}(OMe)_9(NO)_3]$ can be isolated.[43a] It belongs to a different structural type, which notably displays two metal−metal bonds between the four localized Mo(V) centers.

It is noteworthy that in contrast to $[Mo_6O_{18}(NO)]^{3-}$, a reducible type I polyoxoanion, $[Mo_5O_{13}(OMe)_4(NO)]^{3-}$, is expectedly electrochemically inert (no reduction was observed up to −1 V vs SCE) as expected for a type II complex. Moreover, the formation of **II** and **IV** from $[Mo_5O_{13}(OMe)_4(NO)]^{3-}$ does not reflect simple condensation of two units since only one retains its integrity in the products (Figure 3). Thus the formation of reduced decamolybdates probably occurs *via* preliminary degradation of part of $[Mo_5O_{13}(OMe)_4(NO)]^{3-}$, followed by reduction of the resulting fragments and final reaggregation with $[Mo_5O_{13}(OMe)_4(NO)]^{3-}$. The above mechanism is supported by the following lines of evidence: (i) $[Mo_5O_{13}(OMe)_4(NO)]^{3-}$ is known to be unstable in the presence of protons; (ii) $N_2H_4\cdot 2HCl$ was found to be more efficient than $N_2H_4\cdot HCl$ in the formation of blue decamolybdates from $[Mo_5O_{13}(OMe)_4(NO)]^{3-}$, while use of $N_2H_4\cdot H_2O$ led only to a red solution; (iii) while $(n\text{-Bu}_4N)_2[Mo_5O_{13}(OMe)_4(NO)\{Na(MeOH)\}]$ is reduced by [Cp*ReCl$_4$] with formation of blue decamolybdates, the reaction is inhibited in the presence of NEt_3, $(NHEt_3)_3[Mo_5O_{13}(OMe)_4(NO)]$ being the only product isolated in that case;[43b] (iv) increasing the amount of reducing reagent beyond 1 equiv first drops the yield in blue products and finally results in the formation of $(n\text{-Bu}_4N)_2[Mo_6O_{19}]$ exclusively. These observations support degradation of $[Mo_5O_{13}(OMe)_4(NO)]^{3-}$ by protons, either directly introduced or generated by solvolysis of VCl_3 or $[MoCl_4(MeCN)_2]$, prior to reduction. Thus, irrespective of its reducing function, the reducing agent is involved in the degradation of $[Mo_5O_{13}(OMe)_4(NO)]^{3-}$, which should proceed sufficently, although not to completion. Interestingly, it leads to suppose that the nonreduced complex $[Mo_{10}O_{27}(OMe)_4(NO)]^-$ could eventually be obtained by acid−base reactions, which is currently under investigation. Finally, with regard to the formation of the blue decamolybdates from $(n\text{-Bu}_4N)_3[Mo_6O_{18}(NO)]$, it is worth noting that $[Mo_6O_{18}(NO)]^{3-}$ can be transformed into $[Mo_5O_{13}(OMe)_4(NO)]^{3-}$ by reaction with aniline in methanol.[43a]

(43) (a) Proust, A. Doctoral Dissertation, Université Pierre et Marie Curie, 1992. (b) Proust, A. Unpublished results.

Spectroscopic and Magnetic Studies. Only (n-$Bu_4N)_2$**IVa** was obtained in sufficient amount to be adequately characterized by electronic spectroscopy, electrochemistry, and magnetic studies.

The IR spectra of the reduced nitrosyl decamolybdates are deceptively simple. Besides the bands arising from the tetrabutylammonium cations, only three are strong enough to deserve some comments. The band at 1659 cm^{-1} is assigned to the stretching vibration of the nitrosyl ligand and that at 1030 cm^{-1} is associated with the methoxo ligands, while the one at 953 cm^{-1} is attributed to a stretching mode involving the terminal oxo ligands. The intensity of the band(s) with dominant $Mo-O_b$ stretching character is notably low, which is not surprising as both intensity and energy of these bands have been consistently reported to decrease upon reduction.[12c,19,22]

The electronic spectrum of (n-$Bu_4N)_2$**IVa** in acetonitrile solution displays two bands at 635 nm (ϵ = 13 930 mol^{-1} L cm^{-1}) and 920 nm (ϵ = 4600 mol^{-1} L cm^{-1}). Spectra recorded in acetone, dichloromethane, or DMF did not show any significant solvent dependence of the second band, presumably because of its broadness. These data are compared with those for $[W_{10}O_{32}]^{5-}$ (λ = 780 nm, ϵ = 7000 mol^{-1} L cm^{-1}; λ = 1546 nm, ϵ = 4500 mol^{-1} L cm^{-1}, in DMF) and $[W_{10}O_{32}]^{6-}$ (λ = 630 nm, ϵ = 14 000 mol^{-1} L $cm^{-1;}$ λ = 970 nm, ϵ = 10 000 mol^{-1} L cm^{-1}, in DMF).[20,27b,e] Owing to its low energy and its solvent dependence, the band at *ca.*1546 nm has been confidently attributed to an intervalence charge transfer (IVCT) process. Increasing the number of added "blue" electrons is known to result in a blue shift and enhanced intensity of IVCT bands, whereas O → M charge transfer bands decrease in intensity. In view of these observations, we will tentatively assign the band at 920 nm in **IVa** to an IVCT process and the band at 635 nm to the $^2B_2 \rightarrow {}^2E$ d−d transition within localized MoO^{3+} units. Admittedly, the first one is less intense than expected for a four-electron reduced species since the intensity of IVCT bands has been reported to be roughly proportional to the number of "blue" electrons.[1] On the contrary, the second band is by far more intense than expected since the $^2B_2 \rightarrow {}^2E$ d−d transition within a localized MoO^{3+} should be rather weak, and so would be the $^2E \rightarrow {}^2B_2$ d−d transition within the $MoNO^{3+}$ unit (λ = 530 nm, ϵ = 50 mol^{-1} L cm^{-1} for $[Mo_5O_{13}(OMe)_4(NO)]^{3-}$).[32] However, anomalously high intensity of the $^2B_2 \rightarrow {}^2E$ d−d transition is quite common in reduced polyoxometalates and is considered to be caused by intensity-stealing from the nearby IVCT band and by the reduction of symmetry of the M(V) center.[12a]

As expected for a polyoxoanion reduced by an even number of electrons, (n-$Bu_4N)_2$**IVa** is essentially diamagnetic.

Electrochemical Studies. The polarogram of (n-$Bu_4N)_2$**IVa** in DMF, recorded at a rotating platinum electrode between +1 and −1 V vs SCE, displays an anodic wave with $E_{1/2}$ = +0.29 V and a cathodic wave with $E_{1/2}$ = −0.37 V. These values are in agreement with the formal potentials obtained by cyclic voltammetry (Figure 2). The anodic (E_{pa}) and cathodic (E_{pc}) peak potentials for the oxidation process are equal to +0.35 and +0.27 V, respectively, from which a formal potential of +0.31 V is derived. For the reduction process, the mean potential is calculated as −0.40 V from the values for E_{pa} and E_{pc}, −0.36 and −0.44 V, respectively. Both oxidation and reduction processes are quasi-reversible and account for the exchange of a single electron, as is usually the case in nonaqueous solvent. At a dropping mercury electrode, the polarogram of **IVa** displays three reduction processes, with $E_{1/2}$ measured at −0.44, −1.05, and −1.53 V. In the same conditions, the polarogram of (n-$Bu_4N)_4[W_{10}O_{32}]$ displays two

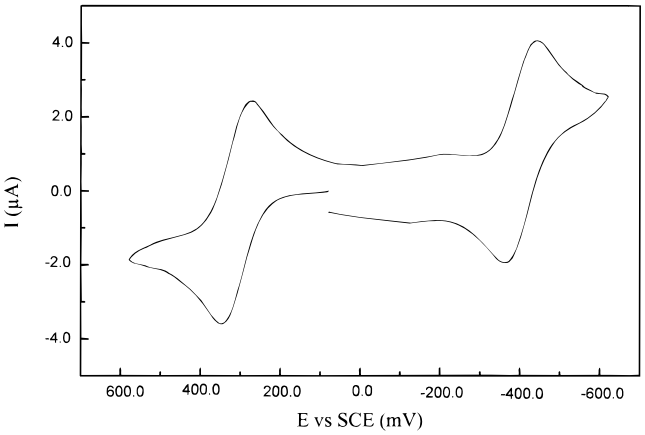

Figure 2. Cyclic voltammogram of (n-$Bu_4N)_2[Mo_{10}O_{24}(OMe)_7(NO)]$ ((n-$Bu_4N)_2$**IVa**) in DMF, at a carbon electrode vs SCE at a scan rate of 0.1 V S^{-1}.

waves at −1.04 and −1.61 V, the height of which are similar to those of (n-$Bu_4N)_2$**IVa** at the same concentration, thus further supporting the monoelectronic character of the processes.

X-ray Diffraction Studies. **II**, **IVa**, and **IVb** crystallize as tetrabutylammonium salts in the monoclinic $P2_1/n$ space group. The asymmetric unit contains one formula entity, that is one anion and either one or two cations. The structures of the anions are depicted in Figure 3: for the sake of clarity, oxygen labels have been omitted (see the Experimental Section for the full numbering scheme).

The overall molecular structure of $[Mo_{10}O_{31-x}(OMe)_x(NO)]^{n-}$ (**II**: x = 6, n = 1; **IVa,b**: x = 7, n = 2) is clearly related to that of $[W_{10}O_{32}]^{4-}$, and these reduced nitrosyl decamolybdates thus provide the first examples of the putative $[Mo_{10}O_{32}]^{4-}$. They can be viewed as composed of two halves of five edge-sharing octahedra each, connected by four nearly linear Mo−O−Mo bridges, with mean angle ranging from 175.1° to 176.3° for Mo−O−Mo angles. In the following discussion, the 10 molybdenum atoms will be divided into two types, axial for Mo1 and Mo101 and equatorial for the eight remaining centers. The Mo2−O23−Mo3−O35−Mo5−O45−Mo4−O24 ring is almost planar with a maximun deviation of 0.07 Å for O23 and O45 in **IVb**, and it is the same for its counterpart in the "lower" subunit of the anion (maximun deviation of 0.04 Å for O123 in **IVb**). The central oxygen atom departures from the corresponding plane range from 0.27 to 0.29 Å for O10 and from 0.19 to 0.22 Å for O110. The larger deviation for the former are very likely attributable to the influence of the Mo(NO) moiety. The structure of the "upper" part of the anions is reminiscent of that of $[Mo_5O_{13}(OMe)_4(NO)]^{3-}$.[32] It accommodates a linear $\{MoNO\}^4$ fragment,[44] formally composed of a Mo(II) center and a NO^+ ligand. Four methoxo ligands and the central oxo ligand O10 complete the coordination sphere of Mo1. Depending on the species under consideration, the "lower" part contains either two or three extra methoxo ligands. In $[Mo_{10}O_{25}(OMe)_6(NO)]^-$ (**II**), the two extra methoxo groups have been found to be distributed among the three sites 113, 114, and 115 (see Experimental Section). The (formal) alkylation of a bridging oxo ligand is expected to result in a lengthening of the Mo−O bonds and in a bending of the Mo−O−Mo unit. This is indeed what is observed, the geometry of O113 being intermediate between those of O112 on one hand and those of O114 and O115 on the other hand. The Mo101−O114 and Mo101−O115 distances of 1.98(1) and 2.05(1) Å,

(44) (a) Enemark, J. H.; Feltham, R. D. *Coord. Chem. Rev.* **1974**, *13*, 339. (b) Feltham, R. D.; Enemark, J. H. *Top. Inorg. Organomet. Stereochem.* **1981**, *12*, 155.

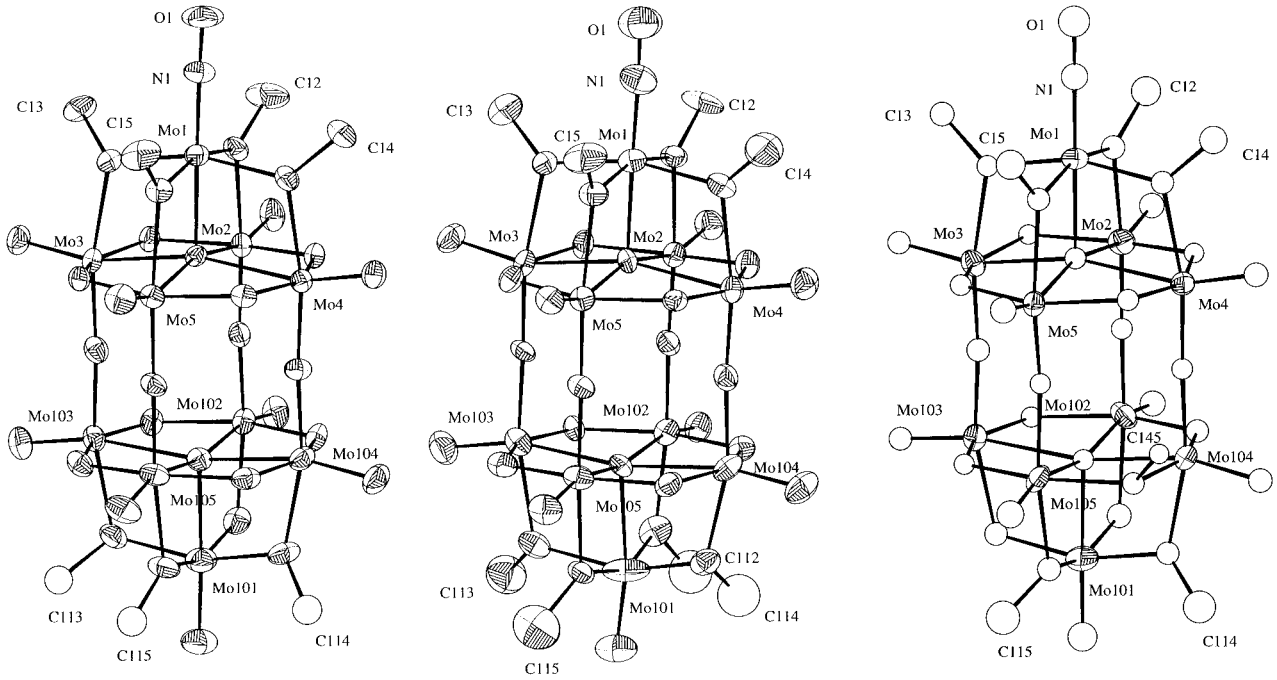

Figure 3. Cameron views of the structures of $[Mo_{10}O_{25}(OMe)_6(NO)]^-$ (**II**) (a), $[Mo_{10}O_{24}(OMe)_7(NO))]^{2-}$ (**IVa**) (b), and $[Mo_{10}O_{24}(OMe)_7(NO)]^{2-}$ (**IVb**) (c). Partial occupation factors: occ(C113) = 0.45, occ(C114) = 0.85, and occ(C115) = 0.70 in **II**; occ(C112) = 0.55 and occ(C114) = 0.45 in **IVa**.

respectively, compare well with the Mo1−O1*i* distances (i = 2−5; mean value 2.00 Å) but are clearly longer than Mo101−O113 (1.91(1) Å), itself longer than Mo101−O112 (1.80(1) Å). Given the standard deviations, the expected trends are less pronounced—although discernible—for Mo10*i*−O11*i* distances and Mo101−O11*i*−Mo10*i* angles (i = 2−5). The O110−Mo10*i* distances of 2.388(9), 2.359(9), 2.288(9), and 2.253(9) Å, for i = 2, 3, 4, and 5, respectively, seem also to reflect the difference in the environments of the Mo10*i* centers. These trends were taken into account in the course of the structure solution to confirm both the location and the occupancy factors of the methoxo ligands and to ensure that no other plausible site had been overlooked; the relevant data are gathered in Table 5. A similar analysis is pertinent to $[Mo_{10}O_{24}(OMe)_7(NO)]^{2-}$ (**IVa**), and the corresponding data are collected in Table 5. **IVa** displays seven methoxo ligands, four in the "upper" part of the anion and three in the "lower". One of the latter is disordered among two sites, namely 112 and 114, with occupancy factors of 0.55 and 0.45, respectively, while the other two are located at sites 113 and 114. A detailed examination of the structural parameters around O11*i* (i = 2−5) clearly reveals that sites 112 and 114 differ from sites 113 and 115. **IVb** differs from **IVa** in the position of the third extra methoxo ligand, which is not disordered this time but located on the *equatorial* site bridging Mo104 and Mo105. Once again, a detailed examination of the geometric features (Table 5) clearly shows that sites 112 and 113 are clearly different from sites 114 and 115, the former being occupied by oxo ligands and the latter by methoxo ligands.

The number of Mo(V) centers in $[Mo_{10}O_{31-x}(OMe)_x(NO)]^{n-}$, *i.e.* the reduction state, leaving the $Mo(NO)^{3+}$ unit aside, can be determined from the values of n and x. The net charge has been deduced from the number of tetrabutylammonium cations. It seems very unlikely that some protons could be involved, at least on sites different from those partially occupied by methoxo ligands, since a careful examination of structural features did not reveal any other distorted site. Thus **II** and **IV** would contain respectively two and four Mo(V) centers. Although x has been determined with very special care, a possible objection is that C112 and C114 still have anomalously large isotropic thermal parameters after disorder treatment in **IVa**, which could suggest that the sum of the occupancy factors on the two sites is less than unity. However, should **IVa** have been a mixture of $[Mo_{10}O_{24}(OMe)_7(NO)]^{2-}$ and $[Mo_{10}O_{25}(OMe)_6(NO)]^{2-}$, it should have been paramagnetic. The observed diamagnetism dictates that the amount of $[Mo_{10}O_{25}(OMe)_6(NO)]^{2-}$, if any, should be small. Another highly speculative description would imply that the unit cell contains $(1 - y)$ methoxo ligand and y hydroxo ligands distributed on the sites 112 and 114, *i.e.* **IVa** would be formulated as $[Mo_{10}O_{24}(OMe)_{7-y}H_y(NO)]^{2-}$. Owing to the lack of experimental evidence for these hypotheses, both **IVa** and **IVb** have been formulated as $[Mo_{10}O_{24}(OMe)_7(NO)]^{2-}$. The bond valence sums calculated by use of $\sum(d/1.882)^{-6.0}$ (d in Å)[45] show some irregular variation, probably because of the disorder. Nevertheless, the average valence sums for the

Table 5. Geometric Distorsions Caused by the Replacement of an Oxo Ligand by a Methoxo Group in $[Mo_{10}O_{25}(OCH_3)_6(NO)]^-$ (**II**)and $[Mo_{10}O_{24}(OCH_3)_7(NO)]^{2-}$ (**IVa**,**b**)

	II	**IVa**	**IVb**
Mo101−O112	1.80(1)	1.89(2)	1.87(2)
Mo101−O113	1.91(1)	2.03(2)	1.89(2)
Mo101−O114	1.98(1)	1.84(2)	1.98(2)
Mo101−O115	2.05(1)	1.99(2)	2.04(2)
Mo102−O112	2.04(1)	2.04(2)	2.07(2)
Mo103−O113	2.07(1)	2.14(2)	2.07(2)
Mo104−O114	2.10(1)	2.07(2)	2.12(2)
Mo105−O115	2.14(1)	2.12(2)	2.10(2)
Mo104−O145	1.90(1)	1.87(2)	1.99(2)
Mo105−O145	1.90(1)	1.87(2)	1.99(2)
O110−Mo102	2.388(9)	2.34(1)	2.47(2)
O110−Mo103	2.359(9)	2.30(2)	2.44(2)
O110−Mo104	2.288(9)	2.38(2)	2.24(2)
O110−Mo105	2.253(9)	2.31(2)	2.24(2)
Mo101−O112−Mo102	115.0(5)	114.9(8)	114.2(9)
Mo101−O113−Mo103	113.2(5)	110.9(7)	113.9(9)
Mo101−O114−Mo104	112.1(4)	114.2(8)	111.3(8)
Mo101−O115−Mo105	112.0(5)	110.6(7)	111.6(9)
Mo104−O145−Mo105			112.1(9)

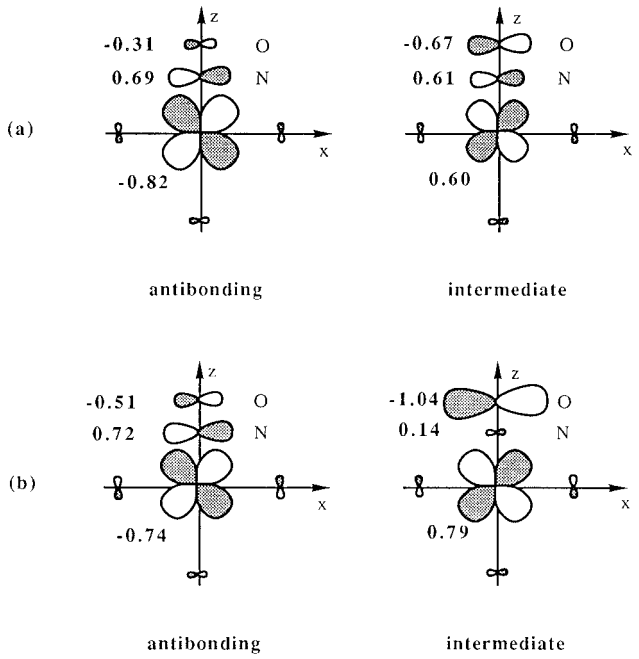

Figure 4. Bonding scheme within the Mo(NO) fragment, derived from EH calculations on $[Mo_{10}O_{25}(OH)_6(NO)]^-$ without charge iteration (a) and on $[Mo(NO)(OH)_4O]^{3-}$ with charge iteration (b). Only the interaction in the *xz* plane is depicted; the bonding MO has not been represented (see text). The unormalized coefficients of the atomic orbitals involved are indicated in boldface.

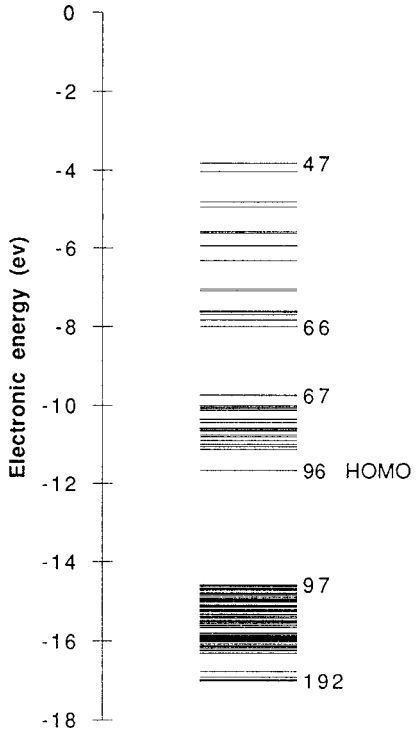

Figure 5. Partial energy diagram resulting from EH calculations on $[Mo_{10}O_{26}(OH)_6]$.

equatorial molybdenum atoms [5.76 in **II**, 5.73 in **IVa**, and 5.63 in **IVb**] are smaller than the values for the lower apical molybdenum atom.

Extended Hückel Calculations. EH calculations have been carried out on $[Mo_{10}O_{25}(OH)_6(NO)]^-$ as a model compound for $[Mo_{10}O_{25}(OMe)_6(NO)]^-$ (**II**). Using the parameters listed in Table 4 without any charge iteration, the calculated MOs were found satisfactory, with the noteworthy exception of those for the Mo(NO) fragment. As stated above, this fragment accommodates four essentially localized d electrons, which are considered to occupy the two degenerate—in C_{4v} symmetry—bonding MOs resulting from the combination of Mo d_{xz} and d_{yz} AOs and the NO(π^*) orbitals. These MOs should have more Mo than NO character, while the opposite is expected for corresponding antibonding MOs. More accurately, the MO pattern within the Mo(NO) fragment involves two degenerate sets of three three-center MOs resulting from the interaction of the Mo d_{xz}, N p_x, and O p_x AOs in the *xz* plane and a similar interaction in the *yz* plane. The coefficient on the central atom (N in this case) in the intermediate MO is usually quite small.[46] The results of our calculations are illustrated in Figure 4a. The bonding MO is not represented because it is diluted among several MOs, owing to the interactions with the polyoxomolybdate framework. Although the interpretation is complicated by the superimposed combination of Mo1 d_{xz}, O13 p_z, O14 p_z, and O10 p_x AOs, it is clear that the intermediate orbital overestimates the contribution of the NO ligand, and more especially that of the central N atom. On the other hand, the contribution of the Mo atom to the antibonding MO is clearly anomalously high. Such inconsistencies presumably arise from the use of inadequate Coulombic integrals for both N1 and Mo1. Thus, to improve the description of the Mo(NO) unit, EH calculations have been undertaken, with charge iteration, on the $[Mo(NO)(OH)_4O]^{3-}$ as a model for the "upper" part of nitrosyl decamolybdates. The resulting values for the Coulombic integrals of Mo1, N1, and O1 are given in Table 6. Those for Mo1 are intermediate between those usually assumed for Mo(0), that is −8.34, −5.24, and −10.50 eV, respectively, for s, p, and d orbitals, and those for Mo(VI) (Table 4). Convergence satisfactorily proved to be independent of the starting set of Coulombic integrals, starting either from those for Mo(0) or Mo(VI). The antibonding and quasi-nonbonding MOs resulting from the combination of Mo1 d_{xz}, N1 p_x, and O1 p_x are presented in Figure 4b. They also reflect the interaction of Mo1 d_{xz} with O13 p_z, O14 p_z, and O10 p_x. Comparison with Figure 4a clearly shows an improvement in the description of the interaction within the Mo(NO) unit.

However, as far as the delocalization of the "blue" electrons is concerned, a complete treatment of the Mo(NO) fragment is not absolutely necessary. Consequently, EH calculations have been carried out on $[Mo_{10}O_{26}(OH)_6]$, as another model compound for **II**, which formally derives from $[Mo_{10}O_{25}(OH)_6(NO)]^-$ by replacement of the $Mo(NO)^{3+}$ unit by a MoO^{4+} unit. A diagram of the calculated electronic energy levels for $[Mo_{10}O_{26}(OH)_6]$ is depicted in Figure 5. It clearly shows that the 224 MOs can be divided into five groups: (i) The first group, below −32.64 eV, includes 32 MOs based on oxygen s-type dangling lone pairs. (ii) The second group, between −17 and −14.57 eV, comprises 96 MOs which are largely localized on ligands. Most of them reflect the σ- and π-bonding mixing of O p and Mo d AOs, while some of them are bonding MOs in connection with O−H bonds and the remaining are nonbonding MOs based on O p lone pairs. (iii) The HOMO, no. 96, belongs to a group of 30 nonbonding or weakly π-antibonding MOs, between −11.67 and −9.74 eV, which are mainly d_{xz}, d_{yz}, and d_{xy} in character. (iv) The fourth group, between −8 and −3.83 eV, is composed of 20 σ-antibonding MOs which are primarily $d_{x^2-y^2}$ and d_{z^2} in character. (v) Above +5.92 eV lies a group of 46 strongly antibonding MOs. Energy values are given to provide an order of magnitude of the gaps between the different groups, although they are questionable, especially for strongly

(45) Brown, I. D.; Wu, K. K. *Acta Crystallogr., Sect. B* **1976**, *32*, 1957.
(46) Albright, T. A.; Burdett, J. K.; Whangbo, M. H. *Orbital Interactions in Chemistry*; Wiley: New York, 1985.

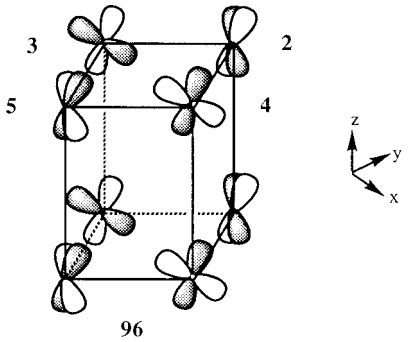

Figure 6. Representation of the HOMO of $[Mo_{10}O_{26}(OH)_6]$.

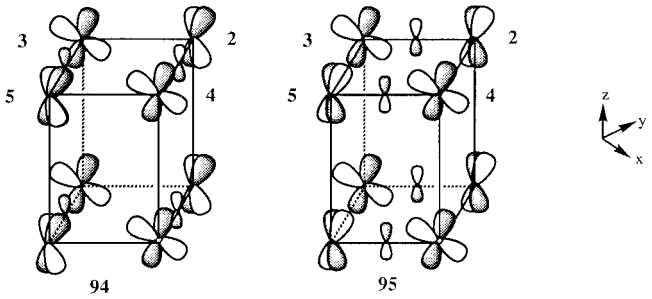

Figure 7. Representation of the doubly-degenerate LUMO of $[Mo_{10}O_{26}(OH)_6]$.

bonding or antibonding MOs. This is an aknowledged limitation of the EH method, which overestimates orbital overlaps.

Let us come back to the group of 30 molecular orbitals containing the HOMO, on which we will more especially focus in the following discussion. The HOMO and the doubly-degenerate LUMO are represented in Figures 6 and 7, respectively. The two electrons in the HOMO are equally and quasi-exclusively distributed among the eight equatorial Mo sites, in d_{xz} or d_{yz} orbitals. The population of these eight d orbitals accounts for "1.92" electrons, the remaining "0.08" electrons residing on the eight O1*i* and O11*i* atoms, 0.01 on each. The HOMO is very slightly antibonding, with an energy of −11.67 eV somewhat higher than the starting value of −12.3 eV for Mo d orbitals. Each component of the LUMO is constructed from eight d_{xz} or d_{yz} orbitals of equatorial Mo atoms, as for the HOMO, but also on four p_z orbitals of four equatorial oxygen atoms of the O_{ij} type. It also comprises, in contrast to the HOMO, a very small contribution of d_{xz} and d_{yz} on both Mo1 and Mo101. As the latter represents only 1.35% of the two electrons which would occupy the orbital, it is hardly significant. Four MOs, namely 96, 91, 79, and 78, display absolutely no contribution of the two axial Mo1 and Mo101 centers. On the other hand, Mo1 and Mo101 AOs always mix with those of the equatorial Mo atoms. However, Mo1 and Mo101, taken together, contribute 66 and 77% of MOs 93 and 92, with the exclusive participation of d_{xy} on both sites. Likewise, MOs 87 and 86 have mainly Mo1 character, while 84 and 83 are mainly Mo101 in character. Six MOs have equivalent contributions of AOs from either axial or equatorial Mo atoms and the remaining 14 MOs exhibit greater involvement of the equatorial sites.

As it seemed nevertheless unsatisfactory to neglect completely the nitrosyl ligand, calculations on $[Mo_{10}O_{25}(OH)_6(NO)]^-$ have been modified. To begin, more accurate energy parameters for Mo(VI) in an oxo environment have been derived by means of EH calculations on $[Mo_{10}O_{32}]^{4-}$, with charge iteration procedures applied to both Mo and O valence shell ionization potentials. The resulting values for Mo are given in Table 6. That for the d orbitals, of −12.62 eV, is close to the starting value of −12.30 eV and as such satisfactory. Calculations on $[Mo_{10}O_{25}(OH)_6(NO)]^-$ were then carried out with the parameters of Table 6 for the Mo(NO) fragment and the Mo centers and the usual parameters of Table 4 for the remaining H and O atoms. Analysis of the frontier orbitals is puzzling, since the four electrons associated with the $\{MoNO\}^4$ fragment would reside in a MO reminiscent of the LUMO of $[Mo_{10}O_{26}(OH)_6]$. This results contradicts the description of the oxonitrosyl complexes as localized (class I) mixed-valence species, as inferred from ^{95}Mo or ^{183}W NMR data on $[Mo_6O_{18}(NO)]^{3-}$ or $[W_6O_{18}(NO)]^{3-}$.[33] The bonding MOs within the Mo(NO) fragment, although correctly depicted, are too high in energy, probably as a result of the differences in energy between formal Mo(II) and Mo(VI) oxidation states.

We did not multiply such calculations in order to adjust the Coulombic integrals and obtain a reasonable bonding description. However, we can draw the conclusion that the introduction of the Mo(NO) moiety into the calculations is not so easily accomplished. Ascribing the same Coulombic integrals to the 10 molybdenum atoms leads to the expected order in the frontier orbitals (two occupied and degenerate MOs resulting from Mo1 d_{xz},d_{yz} and π^*(NO) interactions lying below the HOMO, which accomodates the two extra electrons) but fails to describe correctly the Mo1 d_{xz},d_{yz} and π^*(NO) combinations. In contrast, distinguishing the Mo1 site improves the form of the MOs but leads to an unreasonable energy order. As long as the description of the electronic structure of **II** is restricted to the delocalization of the extra electrons, we will thus content ourselves with the results of the calculations carried out on $[Mo_{10}O_{26}(OH)_6]$.

Discussion

Structural Considerations. Were it not for the nitrosyl and methoxo ligands, the $[Mo_{10}O_{31-x}(OMe)_x(NO)]^{n-}$ anions would approach the D_{4h} symmetry. Although **II** and **IV** are considered to accommodate two and four d electrons, respectively, in addition to those associated with the $Mo(NO)^{3+}$ unit, *i.e.* they could display two or four Mo(V) centers, none of them could be located on the basis of X-ray diffraction data. For the purpose of comparison, mean geometric parameters for $[Mo_{10}O_{31-x}(OMe)_x(NO)]^{n-}$, together with those for $[Mo_5O_{13}(OMe)_4(NO)]^{3-}$ [32] and $[W_{10}O_{32}]^{4-}$,[26] are summarized in Table 7. The Mo···Mo nonbonding distances in **II** and **IV** fall in the expected range for edge-sharing octahedra, with an average of 3.28 Å within the equatorial planes and a somewhat longer value (3.74 Å) between the two equatorial planes. These values compare fairly well with those for $[W_{10}O_{32}]^{4-}$.[26] More generally, the geometric features of **II** and **IV** are very close to those of $[W_{10}O_{32}]^{4-}$,[26] or even to those of $[Mo_5O_{13}(OMe)_4(NO)]^{3-}$,[32] so far as the "upper" part of **II** or **IV** is concerned. Thus it is likely that the structural data for the hitherto unknown oxidized parents of **II** and **IV**, *e.g.* $[Mo_{10}O_{31}(NO)]^{5-}$ and $[Mo_{10}O_{32}]^{4-}$, would be quite similar to those of their reduced derivatives. This is usually the case for the few crystallographically characterized Pope's type I reduced polyoxanions, of which β-$Ca_{0.5}H_6[PMo_{12}O_{40}]$ (4e),[17] β-$[H_4AsMo_{12}O_{40}]^{3-}$ (4e) and α-$[H_2AsMo_{12}O_{40}]^{3-}$ (2e),[18] α-$[HPMo_{12}O_{40}]^{4-}$ (2e) and $[H_3S_2Mo_{18}O_{62}]^{5-}$ (4e),[19] α-$[CoW_{12}O_{40}]^{8-}$ (2e),[47] and $[H_xW_{10}O_{32}]^{4-}$ ($x = 1.5$ or 1.8)[20] are representatives. Detailed comparisons of structural data for "poly blues" with those of their oxidized parents usually reveal only no significant difference apart from a slight expansion in the cluster size upon reduction.[17,48]

(47) Casan-Pastor, N.; Gomez-Romero, P.; Jameson, G. B.; Baker, L. C. W. *J. Am. Chem. Soc.* **1991**, *113*, 5658.
(48) Chen, Q.; Goshorn, D. P.; Scholes, C. P.; Tan, X.-L.; Zubieta, J. *J. Am. Chem. Soc.* **1992**, *114*, 4667.

Table 6. Coulombic Integrals H_{ii} (eV) Derived from Charge Iteration Procedures

	N		O (of NO)		Mo		
	s	p	s	p	s	p	d
$[Mo(NO)(OH)_4O]^{3-}$	−25.05	−12.05	−27.51	−10.91	−8.48	−5.33	−11.14
$[Mo_{10}O_{32}]^{4-}$					−9.51	−6.02	−12.62

Table 7. Comparison of the Main Geometric Features of the $[Mo_{10}O_{25}(OCH_3)_6(NO)]^-$ (**II**) and $[Mo_{10}O_{24}(OCH_3)_7(NO)]^{2-}$ (**IVa**,**b**) Anions with those of $[W_{10}O_{32}]^{4-}$ [a] and $[Mo_5O_{13}(OCH_3)_4(NO)]^{3-}$ [b] Anions

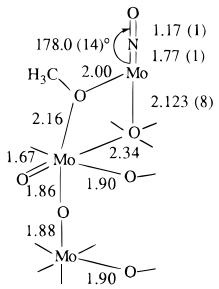

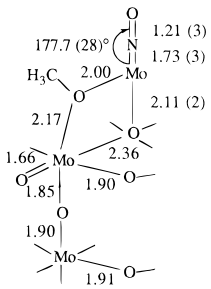

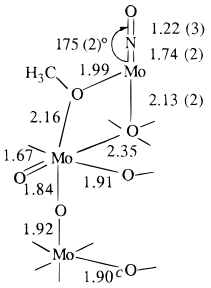

complex	**II**	**IVa**	**IVb**
∠Mo1−O1*i*−Mo*i* (deg)	108.1	107.9	109.1
∠Mo*i*−O*ij*−Mo*j* (deg), $i \neq 1$	119.7	120.4	119.4
∠Mo10*i*−O1*ij*−Mo10*j* (deg), $i \neq 1$	118.5	118.8	120.3[c]
∠Mo*i*−O*i*−Mo10*i* (deg)	175.1	176.1	176.3
Mo1−Mo*i* (Å)	3.37	3.38	3.39
Mo*i*−Mo*j* (Å) *i*, $j \neq 1$	3.29	3.29	3.30
Mo10*i*−Mo10*j* (Å) *i*, $j \neq 1$	3.27	3.28	3.30
Mo*i*−Mo10*i* (Å)	3.74	3.74	3.75

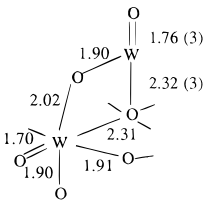

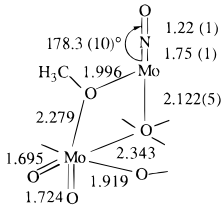

complex	$[W_{10}O_{32}]^{4-}$ [a]	$[Mo_5O_{13}(OCH_3)_4(NO)]^{3-}$ [b]
∠M1−O1*i*−M*i* (deg)	114.3	106.8
∠M*i*−O$_{ij}$−M*j* (deg) $i \neq 1$	117.4	116.2
∠M*i*−O*i*−M10*i* (deg)	175.3	
M1−M*i* (Å)	3.298	3.437
M*i*−M*j* (Å), *i*, $j \neq 1$	3.281	3.257
M*i*−M10*i* (Å)	3.796	

[a] Reference 26 in which the two halves of the anion are related through a mirror-plane. [b] Reference 32. [c] Distances and angle around O145 not taken into account.

The Mo−O distances in **II** and **IV** fall in the expected ranges for terminal and bridging oxo ligands, with mean values of 1.67 and 1.89 Å for Mo−O$_t$ and Mo−O$_b$, respectively. No significant variation in Mo−O$_b$ bond lengths with the Mo−O−Mo angle is observed. Futhermore, the alternation pattern of short and long bonds within the linear Mo−O−Mo bridges found in $[X_2Mo_{18}O_{62}]^{n-}$ anions[49,50] is not observed in **II** and **IV** where the Mo*i*−O*i* and Mo10*i*−O*i* distances are similar. However, the alternation pattern observed in $[S_2Mo_{18}O_{62}]^{4-}$ has been found to vanish upon reduction;[19] thus its absence in **II** and **IV** does not imply that it should not occur in their oxidized parents.

Electronic Structures. An accurate description of the electronic structure of reduced nitrosyl decamolybdates would require a thorough study of these species by a number of spectroscopic experiments, including NMR, ESR, and electronic spectroscopy, in addition to X-ray diffraction. Unfortunately, **II** and **IV** are ESR silent and, furthermore, could not be adequately studied by ^{95}Mo or ^{17}O NMR.

Electron delocalization in mixed-valence complexes is generally assumed to proceed through two main mechanisms:[1,12] electron hopping, the frequency of which strongly depends on the temperature, and electron ground-state delocalization, operating even at low temperatures and relying on orbital mixing. It is well-known that the observed behavior of mixed-valence compounds depends both on the temperature and on the time scale of the spectroscopic technique. The frequency of the thermally activated electron hopping can be obtained from ESR[5,13] and NMR[14,51] data, while the extent of ground-state delocalization can be estimated from ESR hyperfine features. Thermal activation energies have been derived from analysis of ESR line-width temperature dependences for Lindqvist, Keggin, Wells−Dawson, and tungstate Y structures.[5c,d,27e,29,52] Generally speaking, ESR and NMR data for "heteropoly blues" demonstrate that the added electrons are

(49) (a) Stranberg, R. *Acta Chem. Scand.* **1975**, *A29*, 350. (b) D'Amour, H. *Acta Crystallogr., Sect. B* **1976**, *32*, 729. (c) Pope, M. T. *Inorg. Chem.* **1976**, *15*, 2008. (d) Garvey, J. F.; Pope, M. T. *Inorg. Chem.* **1978**, *17*, 1115.

(50) Hori, T.; Tamada, O.; Himeno, S. *J. Chem. Soc., Dalton Trans.* **1989**, 1491.

(51) Barrows, J. N., Pope, M. T. *Inorg. Chim. Acta* **1993**, *213*, 91.

weakly trapped at low temperatures but undergo rapid hopping at room temperature. On the other hand, these electrons appear trapped, even at room temperature, on the shorter time scale of electronic spectroscopy; indeed, electronic spectra of "heteropoly blues" display enhanced d−d bands in the visible and IVCT bands, the intensity of which correlates with the extent of electron delocalization, in the near-IR region. This is typical of class II mixed-valence behavior according to the classification of Robin and Day.[25]

As it might be anticipated, the extent of electron delocalization appears to depend on geometric features, in particular M−O−M angles. It has been found to increase from Lindqvist-type structures, which are constructed only of edge-sharing octahedra (M−O−M = 115°), to Keggin-type structures, which exhibit both edge-sharing and corner-sharing octahedra (M−O−M = 150°)[5c,d] and to Wells−Dawson and tungstate Y structures, which display respectively six and four sets of nearly linear M−O−M bridges. Indeed, an extensive analysis of the electronic spectra of $[W_{10}O_{32}]^{5-}$ according to the PKS model has drawn the conclusion that, although belonging to class II, this complex is very close to class III.[27e] Extensive electron ground-state delocalization in reduced decatungstates is further supported by the disappearance of the O → M charge transfer band in $[W_{10}O_{32}]^{6-}$. The thermal activation energy for $[W_{10}O_{32}]^{5-}$ was calculated to be 0.06 eV.[27e,29] This was first assumed to correspond to an electron transfer between two quasi-linear W−O−W pairs.[27e] However, as this value is almost equal to the value for $[W_6O_{19}]^{3-}$,[5d] it could as well correspond to a hopping process between the equatorial and axial octahedra.[29]

There is now a lot of experimental evidence for electronic delocalization on equatorial sites in Wells−Dawson and decatungstate Y structures. ^{183}W NMR data on 2e-$[P_2W_{18}O_{62}]^{8-}$ were interpreted in terms of electron delocalization on the 12 tungsten atoms of the belts,[14a,b] while the comparison of the *g* values for 1e-$[P_2Mo_{18}O_{62}]^{7-}$ and 1e-$[P_2Mo^{V}W_{17}O_{62}]^{7-}$ also favors delocalization on equatorial sites in the former,[51] as previously inferred from ^{17}O NMR data on 2e-$[P_2Mo_{18}O_{62}]^{8-}$.[53] The comparison of crystallographic data for $[S_2Mo_{18}O_{62}]^{4-}$ and 4e-$[H_3S_2Mo_{18}O_{62}]^{5-}$ reveals that the largest structural changes occur in the belts and so lend futher support for electron delocalization on these sites.[19] The observed hyperfine coupling with eight protons in the single-crystal ESR spectrum of photoreduced decatungstate substantiates electron delocalization, even at 77 K, on the eight equatorial tungsten centers.[54] In addition, ^{183}W NMR data indicate that the two electrons in $[W_{10}O_{32}]^{6-}$ are located primarily on the equatorial sites.[14d]

Since the geometric features of the $[Mo_{10}O_{31-x}(OMe)_x(NO)]^{n-}$ (**II**: $x = 6$, $n = 1$; **IV a**,**b**: $x = 7$, $n = 2$) anions are quite similar to those of $[W_{10}O_{32}]^{4-}$ (*vide supra*), they can confidently be expected to display significant electron delocalization, presumably on the eight equatorial molybdenum atoms. As **IVa**, the only compound that was obtained in a reasonable yield, is diamagnetic, no ESR experiments could be undertaken to obtain an estimate of the thermal activation energy and the extent of electron trapping at low temperatures. Furthermore, ^{95}Mo NMR studies were hampered by the actual low symmetry of the anion and by decomposition in solution. However, EH calculations on $[Mo_{10}O_{26}(OH)_6]$ support electron delocalization on the equatorial Mo sites in **II**. Indeed, the HOMO reflects equal and quasi-exclusive contributions of the eigth equatorial metal centers (Figure 6). However, it must be recognized that EH calculations were carried out in the limit of a class III complex, as the 10 Mo atoms were given the same Coulombic energies, and the structural data were constrained to approximate D_{4h} symmetry. EH calculations at least reveal that electron delocalization, if any, is restricted to the eight equatorial sites and exclude any participation of the axial Mo1 and Mo101 centers, which is consistent with all experimental evidence for the $[W_{10}O_{32}]^{n-}$ system (*vide supra*).

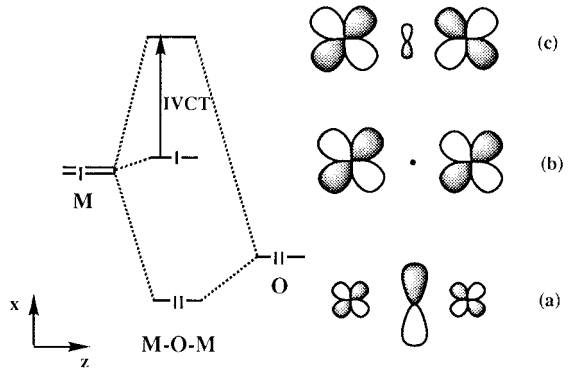

Figure 8. Combination of the M d_{xz} and O p_x AOs in a linear dinuclear mixed-valence complex with a single d-electron.

EH study reports on polyoxometalates are rather scarce.[21,55−60] Those described by Yamase on a fragment of the two-electron reduced $[Mo_{14}O_{46}]^{10-}$ anion[21] are of some relevance to our work, since this study deals with a reduced species including two quasi-linear Mo−O−Mo pairs. Our calculations on $[Mo_{10}O_{26}(OH)_6]$ provide a generalization to a system enjoying four such Mo−O−Mo pairs. Figure 8 represents the bonding scheme resulting from the combination of two M d_{xz} and one O p_x orbitals for a linear M−O−M fragment, holding in a dinuclear mixed-valence complex with one d-electron.[61]

As regards to the form of the HOMO (b), it is clear that the HOMO for Yamase's complex can be viewed as a combination of two b-type MOs, while the HOMO of **II** is constructed of four b-type MOs. The IVCT transition in a dinuclear mixed-valence complex occurs between the b-type HOMO and the c-type LUMO. In this context, it is noteworthy that Yamase found good agreement between the IVCT energy and the calculated gap from the HOMO to an empty MO consisting of two c-type components. In the case of $[Mo_{10}O_{26}(OH)_6]$, 10 MOs from the group including the HOMO, display contributions of the linear oxo bridges. Some of them are quite complex but three are relatively simple: MO 91, which combines only d_{xz} or d_{yz} orbitals of the eight equatorial Mo atoms and p_x or p_y of the four O_i (and some very small contributions on O_{1i} and O_{11i}, as for the HOMO), and MOs 74 and 71, which further involve either the eight terminal oxo ligands O_t, for 74, or the bridging O_{ij} and O_{1ij}, as well as very small amount of Mo1, Mo101, O_{1i}, and O_{11i}, for 71. There are depicted in Figure 9. Although MO 91 appears to be the closest approximation to a c-type MO, its energy relative to the HOMO (0.77 eV) does not match the

(52) Cooper, J. B.; Way, D. M.; Bond, A. M.; Wedd, A. G. *Inorg. Chem.* **1993**, *32*, 2416.
(53) Kazansky, L. P.; Fedotov, M. A. *J. Chem. Soc., Chem. Commun.* **1980**, 644.
(54) Yamase, T. *J. Chem. Soc., Dalton Trans.* **1987**, 1597.
(55) Masure, D.; Chaquin, P.; Louis, C.; Che, M.; Fournier, M. *J. Catal.* **1989**, *119*, 415.
(56) Yamase, T.; Suga, M. *J. Chem. Soc., Dalton Trans.* **1989**, 661.
(57) Moffat, J. B. *J. Mol. Catal.* **1984**, *26*,385.
(58) (a) Jansen, S. A.; Singh, D. J.; Wang, S.-H. *Chem. Mater.* **1994**, *6*, 146. (b) Wang, S.-H.; Jansen, S. A. *Chem. Mater.* **1994**, *6*, 2130.
(59) Calhorda, M. J. *J. Organomet. Chem.* **1994**, *475*, 149.
(60) Gatteschi, D.; Sessoli, R.; Plass, W.; Müller, A.; Krickemeyer, E.; Meyer, J.; Sölter, D.; Adler, P. *Inorg. Chem.* **1996**, *35*, 1926.
(61) Babonneau, F. Doctoral Dissertation, Université Pierre et Marie Curie, 1984.

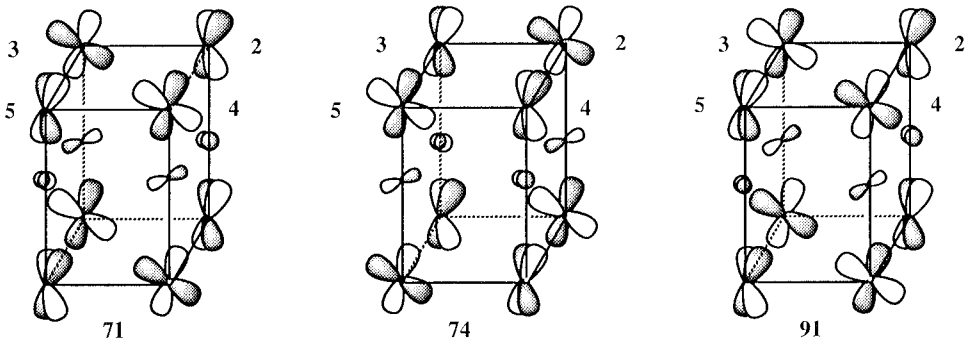

Figure 9. Representation of the orbitals 91, 74, and 71, which might be involved in IVCT.

energy of the IVCT transition (1.35 eV). The energies of MOs 74 and 71, 1.6 and 1.63 eV, respectively, are not more in agreement with the IVCT energy. Furthermore, the transitions from the HOMO to either MO 74 or MO 71 would not be allowed in strict D_{4h} symmetry. However, the calculated energies are strongly dependent upon the starting set of parameters and the actual symmetry of **II** departs from D_{4h}. Furthermore, in contrast to the energy diagram of a dinuclear mixed-valence complex, that of $[Mo_{10}O_{26}(OH)_6]$ displays, above the HOMO, not a single but a bunch of levels potentially involved in the IVCT transition.

Although quantitative discussions of EH are known to be speculative, we might point out that the energy difference between the HOMO and the LUMO (0.53 eV) is not so far, although probably fortuitous, from the difference (0.66 V) in $E_{1/2}$ values for the oxidation and reduction processes observed for **IVa**.

Discussing the magnetic properties of **II** and **IV** in the light of EH calculations is more puzzling. Indeed, examination of the degeneracy of the molecular levels obtained for $[Mo_{10}O_{26}(OH)_6]$ leads to the conclusion that **II** would be diamagnetic with its two "blue" electrons in the nondegenerate HOMO, but that **IV** would be paramagnetic with the two extra electrons in the doubly-degenerate LUMO. However, **IVa** is diamagnetic; this apparent contradiction could arise from the high symmetry imposed on the anion in the calculations, which do not reflect geometric distorsions; a second-order Jahn−Teller effect could also operate. The diamagnetism generally observed for "heteropoly blues" reduced by an even number of electrons is one of the most striking features of this class of compounds, all the more so since, owing to ring currents, reduced compounds are even more diamagnetic than the corresponding oxidized parents.[62] While this behavior has no exception for polytungstates, with susceptibilities neither field nor temperature dependent,[16] ESR signals have been occasionally reported for two-electron reduced Keggin-type molybdates.[63] Spin pairing has long been ascribed to an unusually strong antiferromagnetic interaction *via* a multiroute superexchange.[16] More recently, Tsukerblat has introduced a transfer mechanism of the spin pairing by demonstrating that stabilization of spin singlets can originate from electron transfer processes.[24]

Conclusion

Reduced nitrosyl decamolybdates have been obtained through chemical reduction of $(n\text{-}Bu_4N)_2[Mo_5O_{13}(OMe)_4(NO)\{Na(MeOH)\}]\cdot x$MeOH or $(n\text{-}Bu_4N)_3[Mo_6O_{18}(NO)]$ in MeOH or MeOH/MeCN mixtures. The two-electron reduced derivative $(n\text{-}Bu_4N)[Mo_{10}O_{25}(OMe)_6(NO)]$ ($(n\text{-}Bu_4N)$**II**) and two diastereoisomers of the four-electron reduced $(n\text{-}Bu_4N)_2[Mo_{10}O_{24}(OMe)_7(NO)]$ ($(n\text{-}Bu_4N)_2$**IVa** and $(n\text{-}Bu_4N)_2$**IVb**) have been crystallographically characterized. Complexes **IVa**,**b** differ in the location of some methoxo groups. Spectroscopic characterization of **IVa** and EH calculations on model compounds for **II** have led to the conclusion that these reduced decamolybdates are best described as class II mixed-valence complexes with significant electron delocalization on the equatorial molybdenum atoms. As $[W_{10}O_{32}]^{4-}$ has proved to be an efficient and selective photoinitiator of oxidation of alkanes,[28] the availability of related molybdenum compounds is very attractive. Current efforts are directed toward the electrochemical study of the four-electron reduced derivative. The synthesis and ESR characterization of the three-electron reduced derivatives would complement this novel family of complexes.

Acknowledgment. A.P. is indebted for EH calculations to Prof. D. M. P. Mingos for very kind advice and to Dr. J.-F. Halet for very helpful discussions. This work was supported by the CNRS and the NSF through a joint research program. The work at Syracuse University was further funded by NSF Grant CHE 93/8824.

Supporting Information Available: Tables of atomic coordinates, anisotropic temperature factors, and additional bond lengths and angles for the crystal structures of $(n\text{-}Bu_4N)$**II**, $(n\text{-}Bu_4N)_2$**IVa**, and $(n\text{-}Bu_4N)_2$**IVb** (18 pages). See any current masthead page for ordering and Internet access instructions.

JA9635140

(62) Kozik, M.; Casan-Pastor, N.; Hammer, C. F.; Baker, L. C. W. *J. Am. Chem. Soc.* **1988**, *110*, 7697.

(63) (a) Dorokhova, E. N.; Kazanskii, L. P. *Dokl. Chem.* **1976**, *229*, 489. (b) Kazanskii, L. P.; Fedotov, M. A.; Potapova, I. V.; Spitsyn, V. I. *Dokl. Chem.* **1979**, *244*, 36.